



Review

Novel Processing Methods of Low-Clinker Multi-Component Cementitious Materials—A Review

Paweł Lisowski *  and Michał A. Glinicki * 

Institute of Fundamental Technological Research, Polish Academy of Sciences, Pawińskiego 5B,
02-106 Warsaw, Poland

* Correspondence: plisowski@ippt.pan.pl (P.L.); mglinic@ippt.pan.pl (M.A.G.)

Abstract: The wide use of multi-component cement of highly reduced Portland clinker factor is largely impeded by detrimental changes in the rheological properties of concrete mixes, a substantial reduction in the early rate of cement hardening, and sometimes the insufficient strength of mature concrete. Therefore, major changes are needed in traditional concrete-production technologies if low-clinker cement is to gain wider acceptance. This review's goal is to summarize the impacts of using non-ionizing radiation methods to improve the dispersion of concrete mix constituents, cement setting, and early hardening. The potential impacts of such interactions on the permeability and strength of concrete are also highlighted and investigated. Their intriguing potential for delivering additional energy to cementitious mixtures is analyzed for batch water, solid non-clinker constituents of cement (mainly supplementary cementitious materials), and their mixtures with aggregates. The advantages of adopting these non-traditional methods are found to be highly alluring to the greener preparation techniques used in the construction materials sector.

Keywords: concrete mixing technology; early-age properties; low-clinker multi-component cement; magnetized water; microwave treatment; non-clinker constituents; ultrasound treatment



Citation: Lisowski, P.; Glinicki, M.A. Novel Processing Methods of Low-Clinker Multi-Component Cementitious Materials—A Review. *Appl. Sci.* **2024**, *14*, 899. <https://doi.org/10.3390/app14020899>

Academic Editors: Carlos Thomas, Jose A. Sainz-Aja and Pablo Tamayo

Received: 21 December 2023

Revised: 17 January 2024

Accepted: 18 January 2024

Published: 20 January 2024



Copyright: © 2024 by the authors. Licensee MDPI, Basel, Switzerland. This article is an open access article distributed under the terms and conditions of the Creative Commons Attribution (CC BY) license (<https://creativecommons.org/licenses/by/4.0/>).

1. Introduction

Current developments in construction material technologies are associated with a widespread trend to reduce harmful environmental impacts during the production of materials and their use in buildings and structures. The life cycle analysis of materials in construction elements also covers the issues of the durability of materials—by extending the durability and the service life of structures, the desired effect of reducing the consumption of primary mineral resources can be achieved. Due to the massive use of Portland cement (PC) concrete in construction, the issue of the emissivity of PC cement production has become of great importance. With a simple reduction in the Portland clinker content in cement, whose carbon footprint is estimated at 0.98 kg CO₂/kg clinker (the sum of process, fuel and electricity-related emissions), Gawlicki [1] allows for a substantial reduction in its carbon footprint. Therefore, technologies for the use of cement binders with a highly reduced clinker factor are being developed, using a variety of mineral components or industrial by-products as non-clinker cement constituents [2–5]. In accordance with the European standard EN 197-5 [6], the family of general-purpose cement has recently been expanded to include CEM II/C-M and CEM VI multi-component cement, allowing for an increased proportion of non-clinker main constituents, 36–50% and 51–65%, respectively. In many countries, the range of applicability of new types of cement has not been established yet, and their use is marginal [7,8]. Proske et al. [9] and Chen et al. [10] separately suggested more extreme proposals to limit the content of Portland clinker in cement to 20–35% or even 5%.

The main challenges preventing the greater use of multi-component cement with a low proportion of Portland clinker are related to detrimental changes in the rheological

characteristics of concrete mix, a considerable decline in the early rate of cement hardening, and occasionally insufficient strength of mature concrete. The vulnerability of concrete to variations in ambient temperature and humidity, plastic shrinkage, the phenomenon of bleeding, and increased pressure of the concrete mix on the formwork are all increased by a delayed setting and very slow early hardening of the cement [1–5,11,12].

Moreover, a too-slow increase in concrete strength during the first day following casting restricts, if not outright prevents, the use of the slip-form construction technique; slows the removal and replacement of formwork at the construction site; extends the curing time; and delays other construction tasks that are carried out on already at least partially hardened concrete. Chemical admixtures are a very effective approach to adjusting the workability of the mix and expediting concrete's hardening when used with conventional cement. However, new multi-component cement formulations require the development of specific admixtures for efficient control of the rheological properties of innovative concrete mixtures and their rate of early hardening [1–5,11,12].

Non-clinker constituents of multi-component cement basically consist of supplementary cementitious materials (SCMs) [13,14] that need to be selected and processed properly for their optimal efficiency. The SCMs' fineness, level of clinker replacement, water-to-cementitious-materials ratio, and cement and SCM chemistry (the pozzolanic or hydraulic activity) are only a few of the variables that affect how reactive SCMs are in the cementitious system [13–15]. By modifying the rheological characteristics for a specific application, SCMs, such as granulated blast furnace slag (GGBFS) [16–19], Silica Fume (SF) [16,17,19,20], fly ash (FA) [16,17,21,22], bottom ash [21,23], copper slag [24], volcanic ash (VA) [18], and pulverized fuel ash (PFA) [18], can also increase rheological properties in addition to the mechanical properties and durability of concrete. SCMs may improve concrete characteristics primarily in two ways: by reacting with cement hydration products in the first instance and by improving particle packing efficiency in the second [13–15,25]. Nonetheless, the search for alternative SCMs has significantly intensified in recent years.

In order to use low-clinker cement more widely, significant changes are needed in traditional concrete-production technologies. For the objective of accelerating the early hardening of concrete in precast settings, there are further options to apply hygro-thermal treatment and even gamma irradiation [26,27] (only within radiation-controlled areas). When it comes to multi-component cement with a low clinker content, transmitting heat energy or gamma-ray energy to hardening concrete can also be a method to drive the hardening processes.

Interactions with non-ionizing radiation, such as magnetic interactions, microwaves, and ultrasonic waves, offer exciting possibilities for adding extra energy to concrete mixtures [28]. The potential of ultrasonic waves to carry out detailed diagnostics on the features of hardened concrete and even to demolish concrete is well recognized. Research on concrete constituents and mixtures has occasionally focused on the effects of microwaves, ultrasonic waves, and magnetic interactions. There has not been any published research on the effectiveness of such energy-transmission methods. This study examines non-ionizing radiation technologies to enhance the dispersion of concrete mix components and promote the setting and early hardening processes of cement in concrete. The review also analyses how these interactions affect concrete's early and late strengths, microstructural features, and durability indices that have already been recognized. The applications of low-clinker factor multi-component cement in concrete may be promoted by a clearer grasp of how a non-ionizing radiation field affects constituents of the concrete mix.

2. Ultrasound Treatment (US-T) Methodology

Power ultrasound with a frequency spectrum of 20 kHz–100 kHz finds numerous applications in chemistry and material processing due to its unique properties, which include cavitation, acoustic streaming, and sonochemistry [29–31]. US-T can initiate and accelerate chemical reactions through a phenomenon called acoustic cavitation. The rapid formation and collapse of small bubbles in a liquid (Figure 1) create localized high temperatures

and pressures, leading to enhanced reaction rates and yield. Ultrasonic waves can also disperse and de-agglomerate particles in suspensions, emulsions, and colloidal systems. The cavitation forces break down larger particles into smaller ones, leading to improved stability and homogeneity of the material [29–31].

Cavitation collapse produces deeply felt local heating (5000 °C), high pressures (1000 atm), and heating/cooling rates ($>10^{10}$ °C s⁻¹), thus creating individual conditions for different types of chemical and physical changes [32–37]. The acoustic power, frequency, hydrostatic pressure, the gas used, and reactor shape are only a few variables that may impact acoustic cavitation [32–37]. An intermediate-frequency ultrasound (between 100 and 1 MHz) encourages the production of hydroxyl radicals through regional hot spots caused by cavitation [32–37]. US-T can control crystal size distribution and reduce particle agglomeration due to more stable particles. It can help to direct the course of rapid crystallization processes in which the nuclei are produced due to acoustic cavitation process [33,38,39].

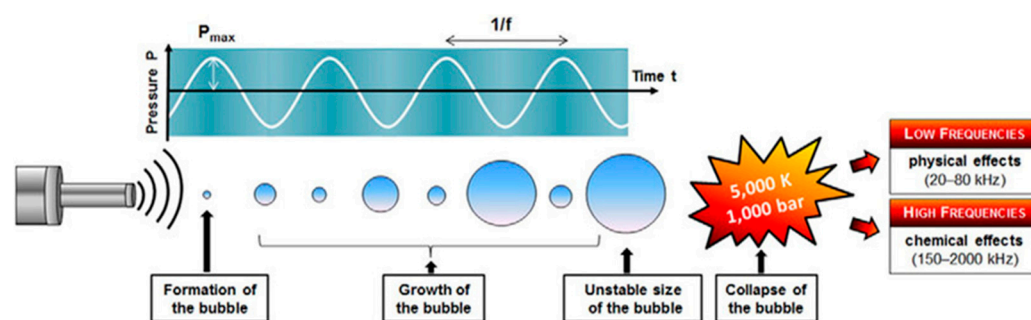


Figure 1. The acoustic cavitation methodology (with permission from [37]).

US-T of Cementitious Materials/Concrete and SCMs

In concrete construction engineering, US-T waves are conventionally employed for the nondestructive diagnostics of structural conditions, including flaw detection or damage development [40–45]; for early-age hardening monitoring to aid technological processes like formwork removal, aggregate exposure, etc. [45–52]; and also for concrete demolition works. Applications of power US-T in construction material processing include the sonochemical activation of natural pozzolans [53].

Power US-T has proven highly beneficial in crystallization procedures, playing roles in seeding, crystal formation, and growth. Cavitation bubbles act as building blocks for crystal development while disrupting the medium and releasing more seeds and nuclei into the solution. Studies involving synthetic calcium silicate hydrate (C-S-H) or nanomaterials in cementitious systems have explored these effects [54,55]. Investigations on CaCO₃ precipitation by Nishida [56] found that US-T enhanced the speed of calcium carbonate precipitation in a supersaturated solution. The most important consideration in these events was macrostreaming, rather than microstreaming, which is typically associated with cavitation. The presence of SCMs agglomerates led to the formation of C-S-H, with a significantly higher calcium-to-silicate (Ca/Si) molar ratio than typical cementitious composites due to microstructural and chemical reactions [57].

US-T application can overcome challenges in the particle hydration of PC and SCMs in concrete technology and cement chemistry, including aggregation/agglomeration, packing density control, and hydration rate control. Hydration mechanisms in PC systems are complex [58], and pore structure has a significant impact on the mechanical characteristics and durability of hardened cement materials [58,59]. The penetration/dissolution of anhydrous phases during hydration plays a crucial role in controlling cementitious materials' early age and long-term properties [58–60]. US-T accelerates the heat release rate during the hydration acceleration phase but does not affect the total heat release [30] (Figure 2). The accelerated strength development in sonicated cement suspensions, observed for the first 16 h, is likely due to rapid cement hydration [30].

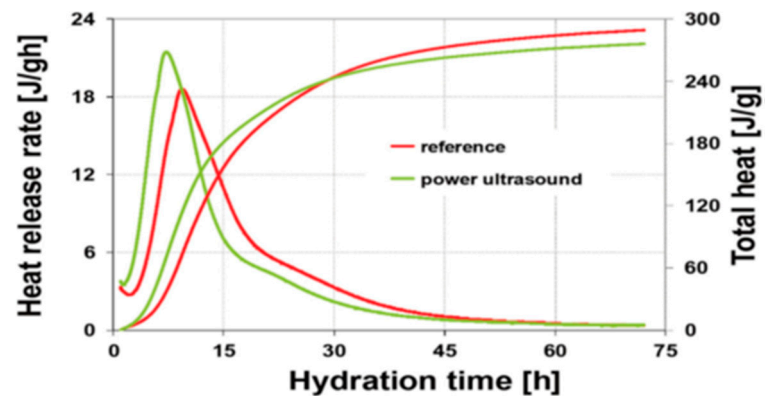


Figure 2. Isothermal heat release rate, reference total heat, and suspension of sonicated cement during hydration (with permission from [30]).

Vaitkevicius et al. [61] introduced a novel method for 3D concrete printing composition using a US-T dispersion apparatus (ultrasonic processor with water-cooled transducer, Figure 3). This method achieved an f_c of 1 MPa at 20 min of hydration and 50 MPa after 28 days, with the freshly prepared mixture transported to the ultrasonic dispersion device within 5 min to avoid premature setting. Ultrasonic dispersion equipment accelerates hydration, making shorter transport times acceptable.

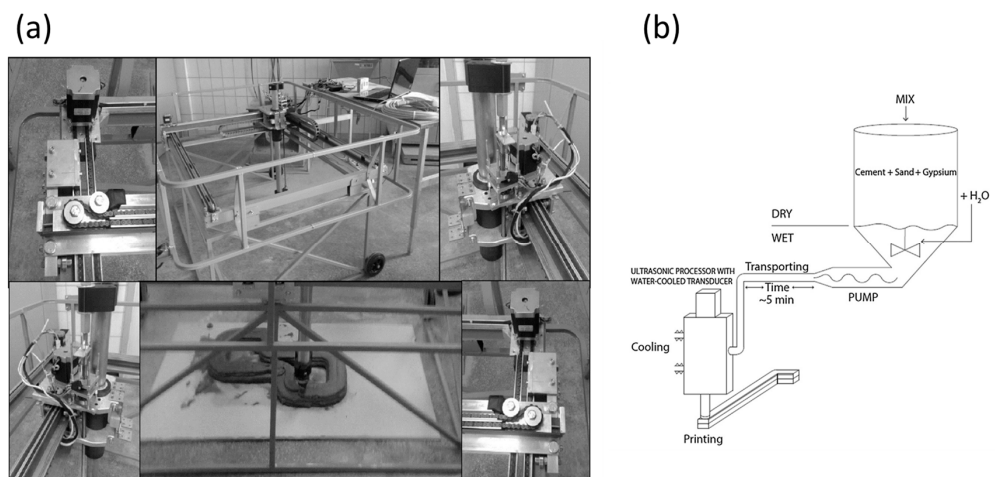


Figure 3. (a) Real photos of the US-T dispersion-based 3D concrete printing system (main parts: stainless steel frame, chain and pulley drive system, and the printing head), (b) schematic diagram of the mixing process and the controlling method for the setting time (with the permission of and recreated using data published in [61]).

Rodríguez et al. [62] showed that after 60 days of curing, mortar containing sonicated Silica Fume (SSF) (a mineral admixture for the PC system) exhibited a significantly higher f_c (over 38.9 MPa compared to non-sonicated SF) and a more than 20% reduction in total capillary porosity with diameters larger than 10 μm . Ultrasonic processing altered the particle size distribution, favoring smaller sizes, resulting in SSF with an average particle size of 3.85 μm , volume content of sub-micrometric particles of 56.9%, and a d_{50} of 0.72 μm . The particle size that corresponds to a 50% cumulative frequency is known as the d_{50} . SSF also demonstrated enhanced pozzolanic reactivity, as evidenced by increased consumption of portlandite during paste hardening. Pastes containing SSF exhibited 68% consumption of portlandite after 28 days of curing, compared to 28% for pastes containing Densified Silica Fume (DSF). The presence of agglomerated SF leads to the production of a calcium silicate hydrate (C-S-H)-type product with a longer chain length structure, higher silicon substitution by aluminum, and a lower Ca/Si ratio after US-T.

A C-S-H phase with a significantly higher Ca/Si ratio than high-performance concrete was observed when SF agglomerates were present [57]. The reflections associated with C-S-H for SSF showed higher intensity, particularly in materials cured for 60 days [63]. Ultrasonic irradiation increased the number of nanometric particles in SSF (up to 90% compared to 22% without US-T), decreased its mean size to reach 57 nm, increased dispersibility, and significantly enhanced the f_c after 28 days of curing (up to 20% with 1% nano-SF). SSF demonstrated higher zeta potential values after 15 min of sonication, indicating high stability and a low propensity to aggregate.

SF can enhance concrete strength, reduce porosity, and extend the usable life of concrete structures. The filler effect of SF impacts the physical but not chemical processes [64,65]. Sonicated SF exhibits higher pozzolanic activity, generating more C-S-H phase [66,67] due to its higher specific surface area.

Another method to increase SF reactivity in PC mortars was described in [68]. The f_c of SSF mortar increased up to 15 MPa after 28 days of curing, especially with longer sonication times (20–25 min) and higher sonication power levels (141 W). SSF showed pozzolanic activity following ultrasonic treatment, resulting in the development of new calcium silicate hydrate (C-S-H, calcium aluminate hydrates, ettringite, etc.) products. Cement paste with SSF exhibited up to 43% less Ca(OH)_2 than with non-sonicated SF after 28 days of curing [69], and SSF was uniformly disseminated into the cement paste (Figure 4). Table 1 indicates the efficiency of the US-T on the reactivity of DSF (DSF-1, DSF-2, and DSF-3) with varying chemical compositions, which are equivalent to sonicated SF (SSF-1, SSF-2, and SSF-3, respectively).

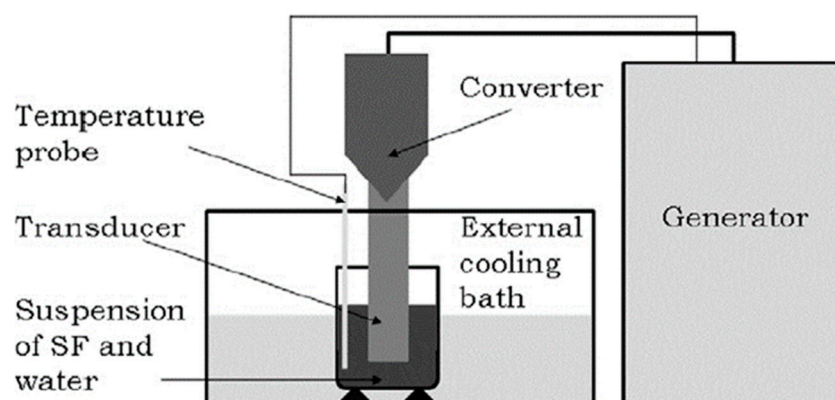


Figure 4. System for US-T of SF (with permission from [69]).

Table 1. Effectiveness of reduction in the content of Ca(OH)_2 through sonication treatment (with permission from [69]).

Reduction of the Content of Ca(OH)_2 by the Sonication Treatment (%)		
SF-1	3 days	22.3
	7 days	28.6
	14 days	43.9
	28 days	35.7
SF-2	3 days	13.9
	7 days	14.7
	14 days	32.9
	28 days	34.1
SF-3	3 days	13.7
	7 days	25.6
	14 days	23.1
	28 days	42.6

Pastes produced with SSF showed up to 43% lower CH content compared to pastes made from untreated SF. Sonication treatment significantly increased SF reactivity, resulting in stronger pozzolanic activity when used as a mineral additive in PC systems. At the early curing stages, SSF-2 and SSF-3 exhibited 14% higher reactivity than untreated SF (DSF-2 and DSF-3), and their reactivity with CH increased with the curing age. After 28 days, pastes with SSF-1, SSF-2, and SSF-3 had 36%, 34%, and 43% lower portlandite content compared to pastes with DSF (DSF-1, DSF-2, and DSF-3, respectively) [69]. Adding SF improves early concrete strength and lowers permeability, serving as both a filler and pozzolan [69]. The hydrated paste with SSF showed an atomic Ca/Si ratio in the range of 1.64–1.83, which is attributed to uniform SSF dispersion and C-S-H formation. The zeta potential of SSF increased significantly (up to 71%) with longer sonication times (up to 8 min), indicating improved suspension stability and SSF de-agglomeration.

The optimization of the sonication time and the solid-to-liquid ratio of nano-silica cement mortars have been proposed by Sharobim et al. [70]. Five minutes of sonication at a solid-to-liquid ratio of 1:10 produced the ideal specific surface area and particle size distribution, leading to a 39% increase in the f_c of nano-silica cement mortar after 7 days and 25% after 28 days compared to the reference material. Nano-silica also enhanced the homogeneity of the cement paste microstructure during sonication and triggered a secondary reaction between SiO_2 and $\text{Ca}(\text{OH})_2$ crystals, resulting in a denser C-S-H phase.

Martinez-Velandia et al. [71] used sonication to alter CSF densification, creating a finer specimen with better granulometric distribution. Commercial SF with an average diameter of 59.6 μm was transformed into samples with an average diameter of about 5 μm and a higher volume percentage of sub-micrometric particles with a diameter of less than 1 μm (over 50%) with longer sonication time (up to 20 min) and higher sonication power level (168 W).

It is important to note that US-T can change the particle size distribution in favor of smaller particle sizes, increase the specific surface area, improve pozzolanic reactivity due to increased consumption of portlandite during paste hardening, achieve a high dispersion (particles uniformly dispersed into cement paste) and degree of de-agglomeration (particles become more stable and have a lower propensity to agglomerate). Additionally, US-T can speed up the heat-release rate during the hydration-acceleration phase. It was also revealed that the rapid cement hydration was what presumably produced the increased strength growth of the sonicated cement suspension, which was only observed for the first 16 h. Especially for SSF treated for longer sonication intervals (20–25 min) and higher sonication power levels (141 W), the f_c of SSF mortar increased up to 15 MPa after 28 days of curing compared to SF prepared without the impact of ultrasound.

3. Magnetic Field Treatment (MF-T) Methodology

Magnetic Field Treatment (MF-T) can improve water's properties by causing the separation of hydrogen nuclei (protons) and water "clusters" into single or smaller molecules due to strong magnetic forces [72–75]. The effectiveness of MF-T depends on the duration of exposure to the MF-T (water flow velocity), magnetic flux density, and volume of water exposed to the field [73,74]. Magnetized water (M-Water) is formed when water passes through a permanent MF-T, leading to molecular structural changes and new characteristics [72,74]. The M-Water layer surrounding cement particles becomes thinner, reducing the need for water during mixing and modifying the physical and chemical properties of M-Water, including surface tension, conductivity, pH, density, volatility, and the ability to alter dissolved substances [73–75]. M-Water also exhibits a lower viscosity than tap water due to a decreased bond angle (from 104.5° to 103°) [72,74,76].

The relationship between MF-T and the surface tension coefficient (σ) of M-Water is not monotonic, as shown in Figure 5 [77]. The optimal MF-T is 300 mT, and both higher and lower intensities lead to an increase in the σ of M-Water, indicating an enhanced magnetization effect. The duration of magnetization varies with the MF-T intensity; stronger MF-T requires shorter treatment times, such as 3 min at 1000 mT and 20 s at 1500 mT [77].

Obtaining M-Water with lower ST is challenging at very high MF-T, and excessive magnetization may even lead to an increase in σ , as reported in Iino and Fujimura's research [78]. The σ of tap water decreases considerably as the treatment duration increases, reaching a minimum of a 9% decline at 13 min with an MF-T of 1000 mT [79].

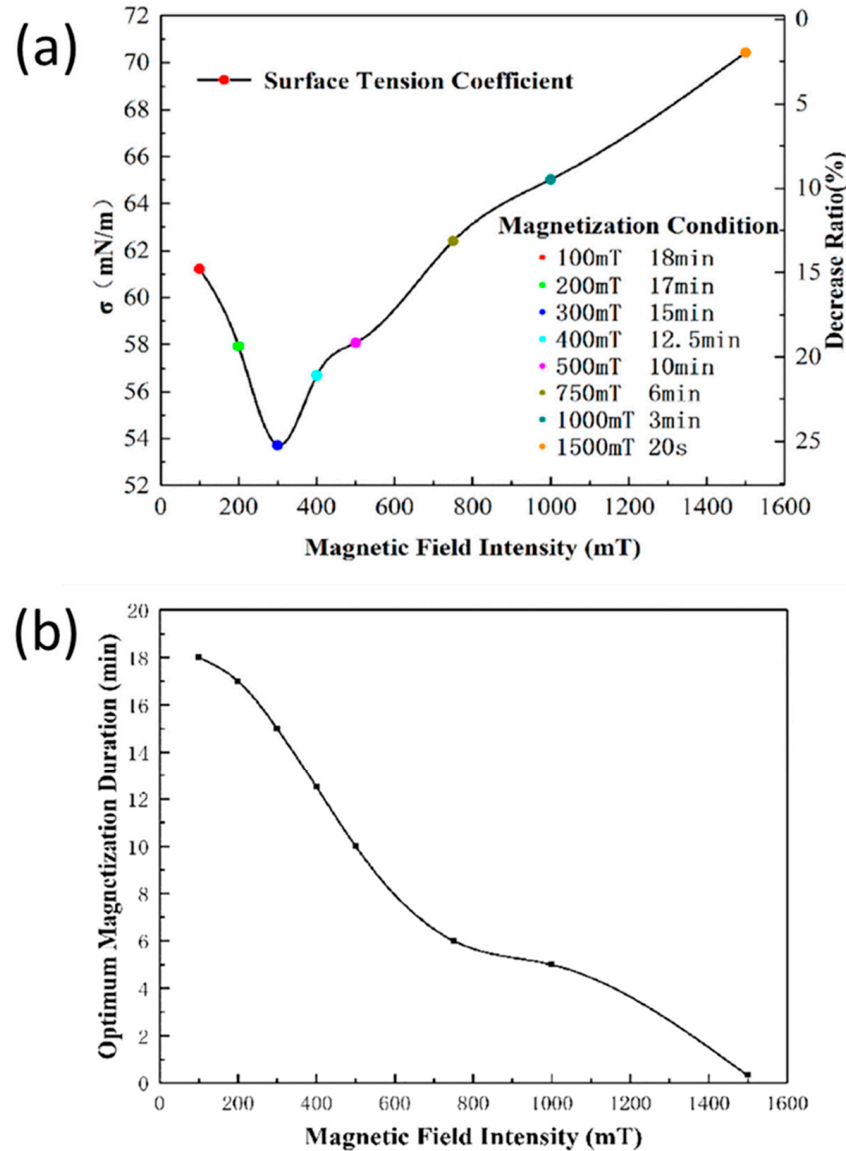


Figure 5. (a) The coefficient of ST of M-Water treated with various MF-Ts; (b) optimal magnetization times for various MF-T (with permission from [77]).

3.1. MF-T of Cementitious Materials/Concrete and SCMs

Ramalingam et al. [72] examined the effects of magnetic water on concrete properties under various magnetic field exposure durations. SEM images reveal the presence of calcium hydroxide ($\text{Ca}(\text{OH})_2$) crystals in cement paste with tap water (Figure 6a) and M-Water (Figure 6b) after 28 days of curing. Specimens prepared with tap water (Figure 6a) included larger CH crystal particles. This is due to the structure of the packing in the transition zone, followed by the cement reaction, which creates clusters of water molecules. The small M-Water molecules react with cement, resulting in the formation of single or smaller molecules. As a result, water activity has improved. At the same time, the hydration process benefits magnetic-field-treated water in a more direct way, which improves concrete efficiency and strength.

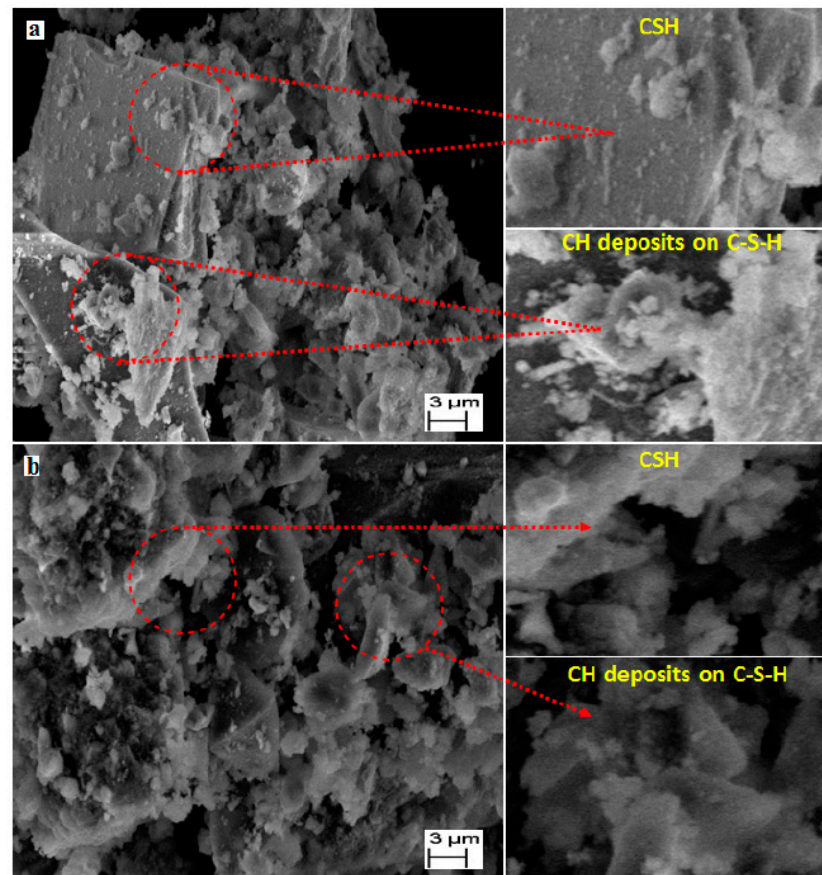


Figure 6. SEM images of calcium hydroxide ($\text{Ca}(\text{OH})_2$) crystals in cement paste prepared with (a) tap water and (b) M-Water (open access status) [72].

The microstructure images of the specimens revealed the presence of CH crystals and fractional voids, while concrete prepared with tap water exhibited larger voids and a lack of CH crystals [72]. Nevertheless, the concrete with M-Water exhibited a higher dispersion of CH crystals and negligible fractional voids, resulting in enhanced structural strength and crack resistance. When M-Water is used in a concrete mix, it allows well water to pass through the cement particles, enhancing the hydration mechanism [72]. The qualities of the concrete mix benefit from improved hydration. It has been discovered that using M-Water in the concrete mix can achieve a high degree of cement hydration and increase concrete strength. The improvement in workability with increasing magnetic field exposure could potentially be related to an increase in Lorentz forces. In this situation, the molecules connected with hydrogen bonds become separated, indicating orbital motion caused by electrons covering the nucleus of water molecules. Subsequently, the O_2^- and H^+ ions are spontaneously expelled from the chemical bond and therefore serving as the primary cause for the heightened activation of the M-Water in a solitary operation. The applied magnetic field exclusively modifies the physical structure of water molecules by changing their shape without impacting individual molecules or smaller entities. Due to the decreased size of water molecules, the layer of water around the cement becomes thinner than usual, leading to a decrease in the amount of water needed to prepare concrete. Simultaneously, the M-Water molecules possess the capability to infiltrate the cement grains, leading to enhanced concrete strength [72].

Recent studies [73–75] indicate that altering the concrete mixing water with M-Water can improve fresh and hardened concrete properties, including water absorption; flexural, compressive, and splitting tensile strength (fst); workability; bleeding characteristics; and resistance to freezing and thawing. The physiochemical and mechanical characteristics of concrete are influenced by solid constituents and the type and quantity of water used

during production [72–75]. Water plays a crucial role in cement setting and concrete hardening through hydrolysis, hydration, and curing stages [75]. Concrete mixed with M-Water exhibits a higher packing density, improving its properties and potentially reducing the impact of chemical additives on cement hydration [72]. M-Water also enhances cement particle dispersion and hydration, leading to higher quality and density in concrete [76,80–82].

Mixing water with cement initiates the hydration process on cement particle surfaces, resulting in the formation of a thin layer of hydration products that hinder further hydration and slow down strength development [79,82,83]. In contrast, utilizing the M-Water system (Figure 7) reduces cement particle agglomeration and enhances the interaction between water molecules and cement particles, leading to efficient hydration and improved mechanical characteristics of concrete [84,85]. Additionally, Wang et al. [86] reported that M-Water penetrates cement granules more easily due to the loose bond between water molecules and single polar molecules (O_2^- and H^+), allowing electrically charged cement particles to move faster. This breaks up cement clusters, making trapped mixing water flow more efficiently and increasing the ST of concrete. The preparation cost of M-Water is low compared to concrete additives, and the mixing procedure is streamlined [74,75]. The impact’s main conclusions from different non-conventional methods on the preparation of low-clinker constituents of cement can be outlined as follows and are shown in Table 2.

Ibrahim et al. [73] observed beneficial effects on the mechanical properties (compressive, flexural, and split tensile strength) of fresh and hardened concrete when using M-Water. Ghorbani et al. [87] found that M-Water significantly improved the microstructure of foam concrete with a 0.75 m s^{-1} magnetizing flow speed. The mechanical properties of concrete were enhanced by M-Water, as evidenced by increases in compressive strength (f_c) of 12.2%, 10.2%, and 8.6% after 7, 28, and 90 days, respectively, and increases in flexural strength of 11.9%, 10.5%, and 9.7% at the same ages, along with increases in split tensile strength (f_{st}) of 10.9%, 9.8%, and 8.5% at the same ages. Ahmed [88] observed a 20% increase in the f_c of concrete mixed with M-Water, which was achieved by carefully selecting parameters such as water flow velocity (0.71 m s^{-1}) and treatment duration (4.5 s per liter). Ghorbani et al. [89] studied the effects of M-Water on self-compacting concrete (S-CC) reinforced with steel fibers. The mixing water was passed via a permanent MF-T (0.65 T) once and 15 times. The steel-fiber-reinforced SCC showed significant improvement in workability, f_c , and f_{st} (50% relative increase after 28 days) compared to control specimens when mixed with M-Water.

Table 2. Summary of effects on hardened concrete properties—the microstructural features, mechanical properties, permeability, and durability indicators (US-T: power ultrasound treatment, M-Water: magnetized water).

Aggregates (F-Fine, C-Coarse)	SCMs/Replacement Levels (%)	Main Findings	Treatment Refs.
Microstructural features, porosity			
F: nonreactive sand	DSF/(5, 10, 20)	- US-T processing altered the particle size distribution, favoring smaller sizes, resulting in SSF with an average particle size of $3.85\ \mu\text{m}$, a volume content of sub-micrometric particles of 56.9%, and a d_{50} of $0.72\ \mu\text{m}$.	US-T [62]
C: crushed limestone F: nonreactive sand	SF/(1, 5, 10)	- US-T can increase the number of nanometric particles in SSF (up to 90% in contrast to the initial SF), decrease its mean size to reach 57 nm, and increase its dispersibility. - SSF’s zeta potential values after 15 min of US-T were significantly higher than those of initial SF, indicating that the particles were highly stable and had a low propensity to aggregate.	US-T [63]
-	DSF/(10) NDSF/(10)	- In comparison to NDSF, the particle size distribution of SSF was found to be less variable, indicating the efficiency of US-T. - The use of US-T to densify SF increases its reactivity through a de-agglomeration mechanism.	US-T [69]

Table 2. Cont.

Aggregates (F-Fine, C-Coarse)	SCMs/Replacement Levels (%)	Main Findings	Treatment Refs.
F: nonreactive sand	SF/(20) NSF/(1, 2, 3)	- Five minutes of US-T at a solid-to-liquid ratio of 1:10 produces the ideal specific surface area and particle size distribution.	US-T [70]
-	SF/(8, 10) NSF/(2)	- The combined US-T of SF and NS leads to a higher porosity decrease and a higher refinement of the large capillary pores in ternary pastes (cement + SF + NSF).	US-T [71]
F: river sand C: crushed limestone	Granite Waste Dust (GWD)/(5, 10, 15, 20)	- The difference in acid resistance between specimens produced with M-Water and those produced with tap water was attributable to the denser structure, which consequently had a lower number of pores and lower porosity.	M-Water [90]
28 days strength, elastic modulus			
F: nonreactive sand	DSF/(5, 10, 20)	- The addition of 10% of DSF results in increases in the fc of up to 36 and 22% compared to the reference specimen.	US-T [62]
-	DSF/(5, 10, 15)	- The fc of SSF mortars is found to be increased by 10 to 15% as a result of US-T in contrast with the control mortar.	US-T [68]
F: nonreactive sand	SF/(20) NSF/(1, 2, 3)	- The fc increased by 39% and 25% after 7 and 28 days, respectively, due to indirect US-T for 5 min at a concentration of 1:10.	US-T [70]
Indigenous C and F aggregates	GGBFS/(5, 15, 25)	- The fc of mortar specimens mixed with M-Water (0.8–1.35 T) increased by 9–19% compared to those mixed with tap water.	M-Water [83]
Indigenous C and F aggregates	FA/(5, 10, 15)	- The fc of the mortar specimens improved from 15% to 20% when the MF-T was 0.8 or 1.2 T.	M-Water [84]
F: river sand C: crushed gravel	SF, metakaolin, rice husk ash, FA/(10, 20)	- After 28 days, fc and fst increased up to 49% and 41%, respectively, while the water-absorption value decreased up to 55%; an SCC combination including M-Water and 20% SF can be regarded as an optimum mix design.	M-Water [85]
F: river sand C: crushed limestone	GWD/(5, 10, 15, 20)	- After 28 days, the fc of specimens prepared with M-Water and 0%, 5%, 10%, 15%, and 20% GWD improved by 7%, 8%, 8%, 10%, and 11%, respectively, compared to specimens prepared with tap water.	M-Water [90]
Indigenous C and F aggregates	Limestone powder (10)	- Compressive, bending, and tensile strengths of the concrete produced increased by up to 34.1%, 52.4%, and 74.2%, respectively.	M-Water [91]
F: river sand	Marble waste dust (MWD)/(10, 20, 30, 40)	- After 28 days of curing, mortar mixes containing M-Water and 0%, 10%, 20%, 30%, and 40% MWD showed, respectively, significant fc improvements of 32%, 21%, 17%, 26%, and 6% in the CS of the mortar mixes. - The 28-day tensile strength test of mortar specimens with 10%, 20%, 30%, and 40% MWD was enhanced, respectively, by using M-Water by about 11%, 5.5%, 16%, 3%, and 5%.	M-Water [92]
F: siliceous natural sand C: crushed stone	Egyptian nano- Al_2O_3 (EN-Al)/(1, 2, 3)	- When 0, 1, 2, or 3% of EN-Al replacement levels were used, there was an increase of about 8, 12, or 16% in the 28-day fc of specimens made with M-Water compared to specimens made with tap water.	M-Water [93]
F: volcanic particles C: volcanic rock	VA (0, 5, 10, 15, 20)	- The fc of concrete is increased by 24% after 7 days when 5% of VA and tap water are added.	M-Water [94]
F: river sand C: lightweight expanded clay	SF/(5, 10) GGBFS/(10, 20)	- The fc of concrete is increased by 24% after 7 days when 5% of VA and tap water are added.	M-Water [95]

Table 2. Cont.

Aggregates (F-Fine, C-Coarse)	SCMs/Replacement Levels (%)	Main Findings	Treatment Refs.
		Permeability, durability indicators	
F: nonreactive sand	DSF/(5, 10, 20)	- SSF prepared using US-T demonstrated enhanced pozzolanic reactivity, as evidenced by increased consumption of portlandite during paste hardening. Pastes containing SSF exhibited 68% consumption of portlandite after 28 days of curing, compared to 28% for pastes containing DSF.	US-T [62]
-	DSF/(10) NDSF/(10)	- After 28 days of curing, SSF had up to 43% less Ca(OH) ₂ than non-sonicated SF.	US-T [69]
-	SF/(8, 10) NSF/(2)	- The C-S-H Ca/Si ratio is noticeably reduced using the US-T of SF and NS in the ternary paste (cement + SF + NSF), while the C-S-H MCL is increased, which in turn can improve the durability of the prepared specimens. - After 28 days of hydration, the synergistic effects of ternary paste may help to accelerate the pozzolanic response (lowest CH index).	US-T [71]
F: river sand C: crushed gravel	SF, metakaolin, rice husk ash, FA/(10, 20)	- The amount of high-range water needed for SCC can be decreased by up to 45% with M-Water. - M-Water can reduce SCC's water absorption by up to 10% when compared to the SCC control mix prepared with tap water. Additionally, this value can be decreased by up to 55% for SCC containing 20% SF and M-Water.	M-Water [85]
F: river sand C: crushed limestone	GWD /(5, 10, 15, 20)	- In comparison to specimens prepared with tap water, those prepared with M-Water showed lower water absorption, lower mass loss, and higher resistance to aggressive environments (5% by weight NaCl and H ₂ SO ₄ solutions).	M-Water [90]
Indigenous C and F aggregates	Limestone powder (10)	- The most beneficial benefits of M-Water were seen for electromagnetic field intensity of 1.2 T and a water flow rate of 9 L min ⁻¹ , resulting in a reduction of up to 34.1% in superplasticizer use.	M-Water [91]
F: nonreactive sand	MWD /(10, 20, 30, 40)	- When using 0%, 10%, 20%, 30%, and 40% MWD in comparison to mortar mixes prepared with tap water, respectively, mortar mixes made with M-Water showed lower mass losses of 26%, 36%, 22%, 28%, and 28%. - In comparison to the mortar specimens prepared with tap water, M-Water reduced the water absorption of the mortar specimens by roughly 15%, 14%, 3%, 9%, and 9.5%, respectively. - In comparison to cement pastes prepared with tap water at the same replacing ratios, the initial setting times of cement pastes prepared with M-Water and 0%, 10%, 20%, 30%, and 40% MWD were, respectively, around 8.70%, 7.85, 2.85, 4.25%, and 4.40% longer.	M-Water [92]
F: river sand C: lightweight expanded clay	SF/(5, 10) GGBFS/(10, 20)	- M-Water decreased the slump flow time by an average of 17% while increasing the final slump flow diameter of all the mixes by roughly 9%.	M-Water [95]
F: silica sand C: siliceous aggregate	SF/(5, 15)	- When M-Water is used instead of tap water, the binding strength is increased at the 7- and 28-day curing ages with various bar diameters. - The bond strength of specimens with SF combined with M-Water is greater than that of specimens with the same SF content mixed with tap water.	M-Water [96]

“-“ denotes no aggregate present, i.e., cement paste.



Figure 7. System for M-Water (with the permission of and recreated using data published in [77,87,91]).

The influence of M-Water as mixing water on the f_c , workability, and required cement content was studied by Al-Maliki et al. [97]. Water treated with a 1.3 T MF-T intensity showed the greatest increase in concrete f_c . Ahmed and Manar [98] conducted experimental studies on static MF-T on prepared mix concrete (Figure 8), showing slump increases ranging from 7% to 26%, with the best slump increase for fresh concrete corresponding to 400 mT of MF-T (26% higher).

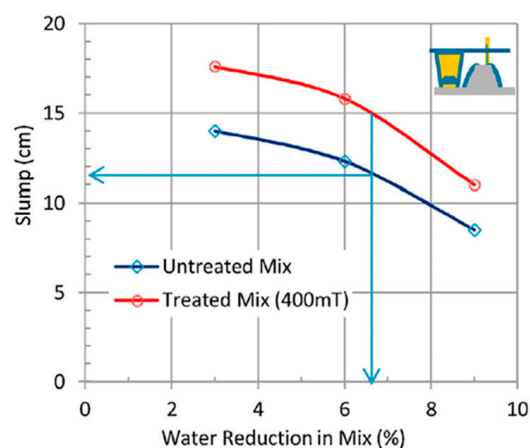


Figure 8. Water-reduction potential due to static MF-T on fresh concrete (open access status) [98].

M-Water mixed concrete showed 30% and 16% increased compressive and splitting strengths, respectively, with enhancement directly influenced by MF-T length. The penetration of M-Water into cement particles during hydration improved activity and resulted in more crystalline hydration products, denser microstructure, and improved concrete performance, including shrinkage cracking resistance. Ebrahimi Jouzdani and Reisi [91]

observed that M-Water in S-CC reduced the use of superplasticizer by up to 34.1% and improved compressive, bending, and tensile strengths by up to 34.1%, 52.4%, and 74.2%, respectively (Figure 9).

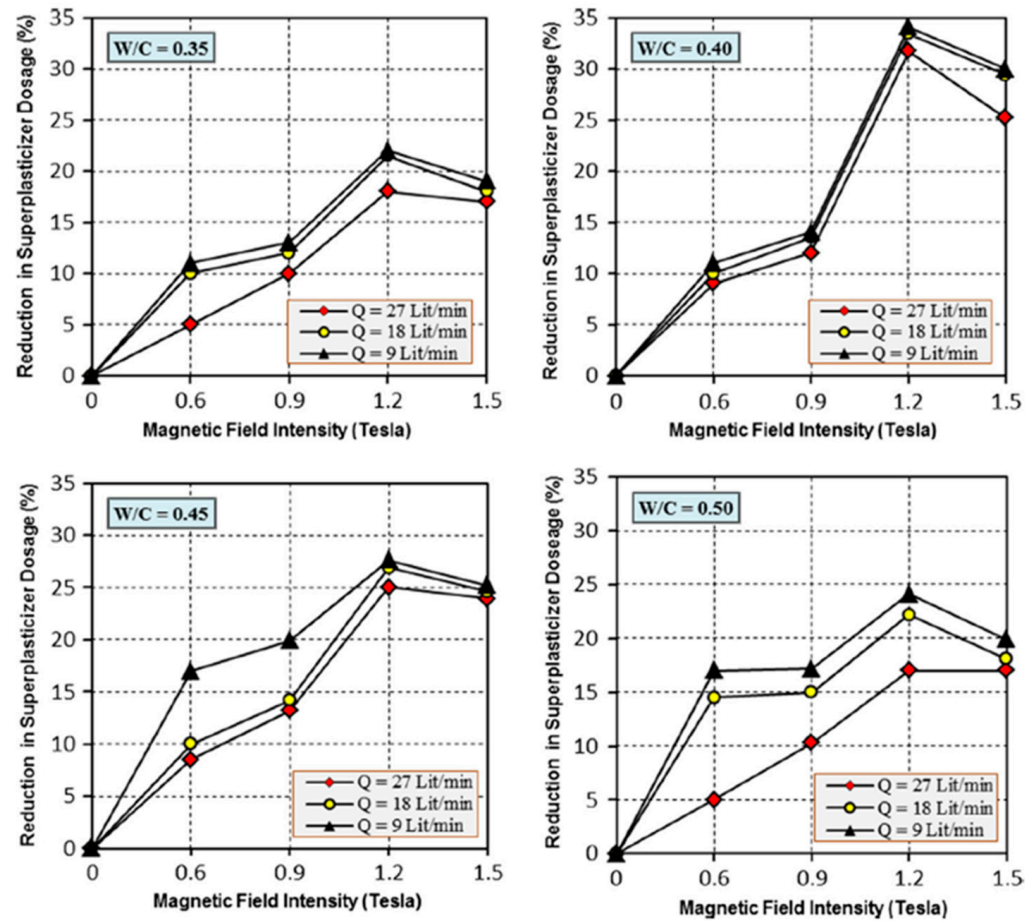


Figure 9. Impact of the properties of M-Water on the amount of superplasticizer dosage reduction (with permission from [91]).

The strength development of concrete under various curing conditions was compared by Ngene et al. [99] using M-Water and untreated water. M-Water resulted in concrete with a 10% higher f_c than regular concrete after 28 days. Wei et al. [100] studied the early-age shrinkage cracking resistance of M-Water mixed concrete, finding optimal performance at 260 mT MF-T, 280 mm MF-T length, 0.8 m s^{-1} water flow, and a 72.2% reduction in total cracking area per unit specimen area.

3.2. MF-T of Mineral Admixtures

Su et al. [83] demonstrated that M-Water increased the f_c of concrete and mortar containing GGBFS by 9–19% depending on the MF-T intensity used for M-Water (0.8, 1.2, or 1.35 T). A similar study by Su et al. [84] revealed an improved f_c in concrete and mortar containing FA mixed with M-Water, with the best results at 0.8–1.2 T MF-T. Gholhaki et al. [85] found that M-Water, combined with 10 or 20% pozzolanic materials (SF, metakaolin, rice husk ash, and FA), enhanced the flowability and viscosity of S-CC. At the age of 28 days, when f_c and f_{st} had increased by 49% and 41%, respectively, the water absorption had decreased by 55%.

In another study, Ghorbani et al. [90] examined the use of GWD as a partial cement substitute in concrete. Up to 10% GWD replacement increased concrete strength, but higher percentages reduced strength and durability. Regardless of the GWD ratio, M-Water led to

reduced water absorption compared to tap water. The effect of M-Water on mortar mixes containing MWD as a partial cement substitute was investigated by Ghorbani et al. [92]. The best performance was observed with 10% marble dust replacement, while higher amounts resulted in reduced strength and durability due to increased porosity.

Ahmed [93] studied the use of EN-Al as a cement substitute in concrete and found that M-Water improved the strength (13%) and reduced the capillary porosity (27%) for specimens with 1% EN-Al. The properties of concrete with VA and M-Water were evaluated by Keshta et al. [94]. M-Water improved the workability and increased the f_c by 43% at 7 days and 36% at 28 days without VA and by 22% at 7 days and 33% at 28 days with 5% VA. The addition of M-Water improved both the workability and the strength, allowing for more environmentally friendly concrete using less cement.

Salehi and Mazloom [95] presented the fracture behavior of self-compacting lightweight concrete (S-CLC) with different cement replacement materials. M-Water improved the fracture energy, fracture toughness, tensile strength, and f_c . Barham et al. [96] examined the impact of M-Water and SF content on concrete's f_c and bond strength. A 5% SF level resulted in the highest f_c and bond strength, while higher SF levels led to strength loss. M-Water increased bond strength with different bar diameters by enhancing the concrete fluidity and reducing the void content.

4. Microwave Treatment (MW-T) Methodology

Microwave treatment (MW-T) is the term for non-ionizing electromagnetic radiation with wavelengths between 1 mm and 1 m and spatial frequencies between 300 MHz (100 cm) and 300 GHz (0.1 cm) [101–104]. By rapidly attenuating MW-T through the intense vibration of polar molecules, it can increase the temperature of the material and accelerate chemical reactions. The entire specimen becomes heated as a consequence of the movement and friction this causes between molecules [104–109]. The frequencies of 915 MHz and 2450 MHz are currently mostly used on cement and concrete for industrial and scientific objectives [110]. Microwaves interact with matter more sensitively than ultrasonic and electromagnetism, which can penetrate dielectric materials and convert electromagnetic energy into heat energy without needing to first warm up a heating cavity. Microwave-absorbing materials generate volumetric heat as a result of the interaction between propagating waves [111–113]. Short reaction times, easy control, improved reaction kinetics, reduced heat loss, clean heating processes, good energy efficiency, and environmental protection are only a few advantages of MW-T over conventional heating techniques [48,109,114,115]. These heating qualities make it possible to cure concrete in an eco-friendly way.

Precast concrete, in particular, has undergone heat curing to expedite the development of strength [48,116]. The skin effect, which is produced by conventional heating methods and is more efficient for surface heating [101], is the fast evaporation of water from treated materials' exterior surfaces. It is difficult to accomplish consistent heating because of the steep temperature gradient, and heated materials lose a large amount of energy through heat conduction and convection.

In contrast, MW-T may promote a temperature rise as a consequence of the polar molecules' ability to absorb heat and form localized heating spots that are independent of position, which is beneficial to generating uniform volumetric heating [104–107,117]. The utilization of MW-T is based on the internal energy loss associated with the stimulation of molecular ions and dipoles under electromagnetic fields [118]. The specimens' microwave heating characteristics can be varied by the secondary material's propensity to absorb, transmit, or reflect MW-T [119]. It has been proven that microwave-assisted heating can cut processing times and lower the expenses of additive manufacturing [104–108,120,121]. Combining these approaches for the best materials processing could be plausible (Figure 10), and it would follow the properties of power ultrasound, microwave, and magnetic processing stated in the preceding chapters.

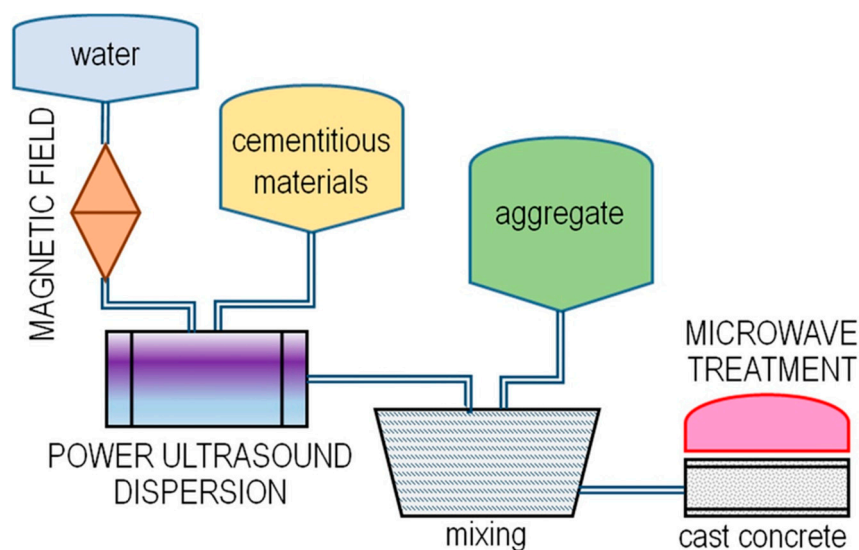


Figure 10. Schematic of a hypothesized approach that would combine magnetic field, high-intensity ultrasound, and microwave processing to produce concrete with increased homogeneity and enhanced early strength.

4.1. MW-T of Cementitious Materials/Concrete and SCMs

Because of its significant benefits of non-contact heating, volumetric and selective heating, user-friendly control, clean heating processes, and no formation of secondary waste, MW-T has recently received much attention [104–108,120,121]. Unfortunately, this may significantly impede the implementation and advancement of such technology in the pavement engineering of the typical cement concrete’s low microwave absorption efficiency, which may reduce the microwave heating speed [104–109,122]. According to research on the electrical field curing approach, C-S-H products’ electroosmotic swelling occurs, and pore connectivity decreases in a DC field [123,124].

Most of the studies mentioned concentrated on using microwave absorbents and absorption aggregate to increase the MW-T efficiency of cement and concrete. This makes it possible to increase the effectiveness of microwave heating of cement concrete in applications like accelerated concrete curing [125], road de-icing [122,125], asphalt concrete repair [125], and the high-performance nondestructive testing of cement and concrete structures [119] with a low cost, a wide range of sources, and excellent performance.

Microwaves can be partially absorbed by dielectric components contained in concrete, boosting temperature and hastening cement hydration. Additionally, mixed water that has been bound in cement hydrates is microwave-resistant. In contrast to heat curing, the hydrates are less easily decomposable. Because it is prone to MW-T, water is necessary for the heating process [126–128]. In turn, concrete quality might improve. As a result, microwave energy is suitable for accelerating the early hardening of concrete and mortar mixes. Because it employs electrical energy rather than combustion, which requires more time and energy, it might be called an environmentally beneficial, green, and clean technology [111,112].

Microwave curing may modestly increase the total porosity of mortar [129] when compared with normal curing and steam curing at 80 °C (under different curing regimes at the age of 28 days). To better understand mortar pore size distribution under various curing regimes, Figure 11 shows four size ranges [129]: large capillary pores (>100 nm), middle capillary pores (50–100 nm), mesopores (4.5–50 nm), and gel micropores (<4.5 nm). It can be stated that MW-T curing may reduce the pores in the range of >100 nm.

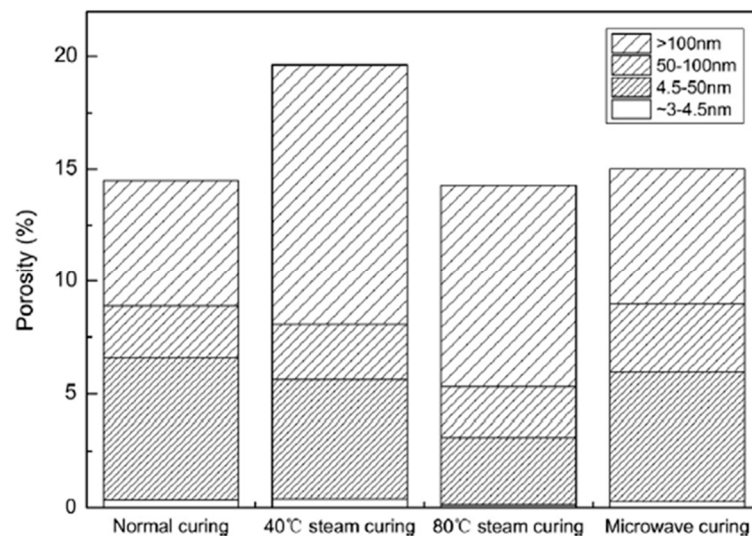


Figure 11. The porosity of mortar under different curing regimes (with permission from [129]).

Different power dissipations are produced by the microwave electromagnetic field's interactions with the constituents of concrete in the MW-T of concrete [119]. Due to varying scales, porosity, aggregates with different mineral compositions, and moisture migration, the distribution of dielectric losses is uneven as microwave radiation is transformed into heat energy inside concrete [103,111,112]. Additionally, rather than only being a thermal-mechanical coupling problem, the MW-T of concrete is a multi-field coupling and multi-phase mixed nonlinear problem. Compared to traditional steam heating, MW-T can speed up the curing process and boost the early strength of concrete [120,128,130]. When exposed to such an electromagnetic field, the dielectric components of concrete vibrate and resonate with the applied field. These interactions prevent the vibration that microwaves cause, which leads to internal friction heating the concrete [130,131].

Xiao et al. [132] investigated the temperature distribution for concrete structures under different heating parameters of MW-T in the diagonal direction (Figure 12). The electric field concentration in the center and surface heat loss from convective heat transfer between the air and the surface are responsible for the observed trends of the lowest temperature at the edge and the highest temperature near the center. A small variation might be ascribed to the unequal composition of the concrete in the cross-section for various specimens. Furthermore, as opposed to rapid MW-T, the delay in heat conduction also increases the temperature differential between the center and the surface. The overall temperature was higher in the heating scheme with the higher maximum temperature. In light of this, a higher temperature of the concrete structure on average will arise from a higher maximum temperature.

Because of the wide variances in their dielectric constants, which cause differences in their thermal responses, the microwave heating sensitivity of aggregate and cement paste are likewise highly different from one another. Separating the aggregates and mortar in concrete happens instantly once the microwave power reaches a particular level. This feature can be very useful for the beneficiation of the recycled concrete aggregate because its adverse effects on the ST of concrete can be attributed to the excessive content of the attached mortar [133]. Concrete mortar–aggregate separation using MW-T outperforms conventional heat treatment techniques [119,128–131]. Since it can increase the amount of electromagnetic energy converted to thermal energy, the temperature difference at the mortar–aggregate interfaces can increase the microwave input power [104–108,128–131]. When MW-T is applied to freshly laid concrete, water is removed, capillary pores close, and the material becomes denser. Although most microwave radiation is used to cure concrete, the radiation period is typically lengthy (more than 1 h with high power) [134]. In terms of effective temperature control, the occurrence of cracks owing to shrinkage, the surface

condition of concrete after curing, economic efficiency, and CO₂ emissions, microwave heat curing performed superiorly to traditional steam curing [135]. However, verification and augmentation based on actual data are required to produce environments suitable for the varied sizes and shapes of forms.

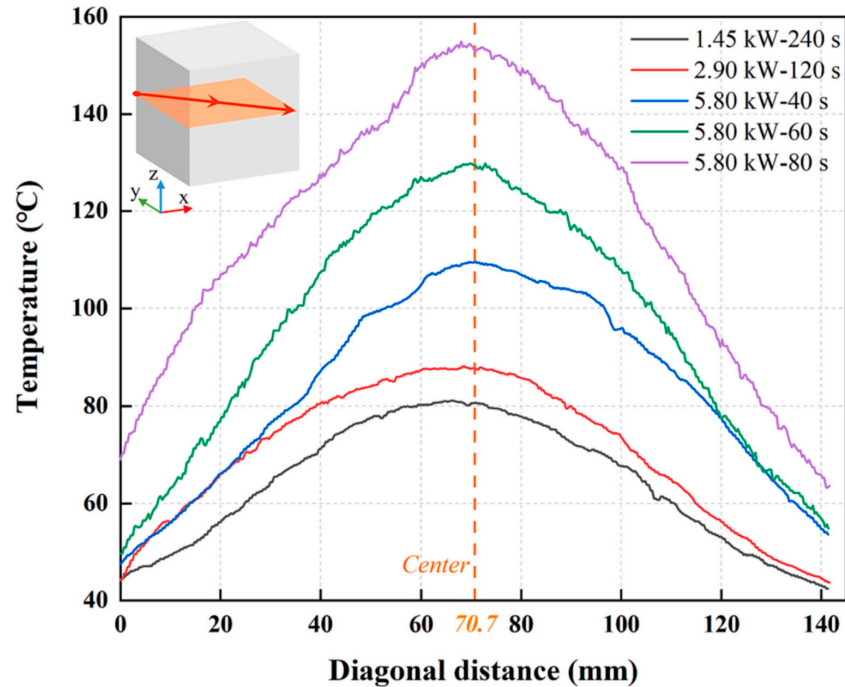


Figure 12. Cross-sectional temperature profile measured at various MW-T in the diagonal direction (with permission from [132]).

In their investigation of the impact of MW-T as a substitute for steam curing on the preparation of concrete, Choi et al. [135] found that using microwaves can result in excellent performance in terms of preventing concrete bleeding, preventing surface separation after MW-T, reducing CO₂ emissions, and saving energy costs when compared with conventional preparation systems (Figure 13).

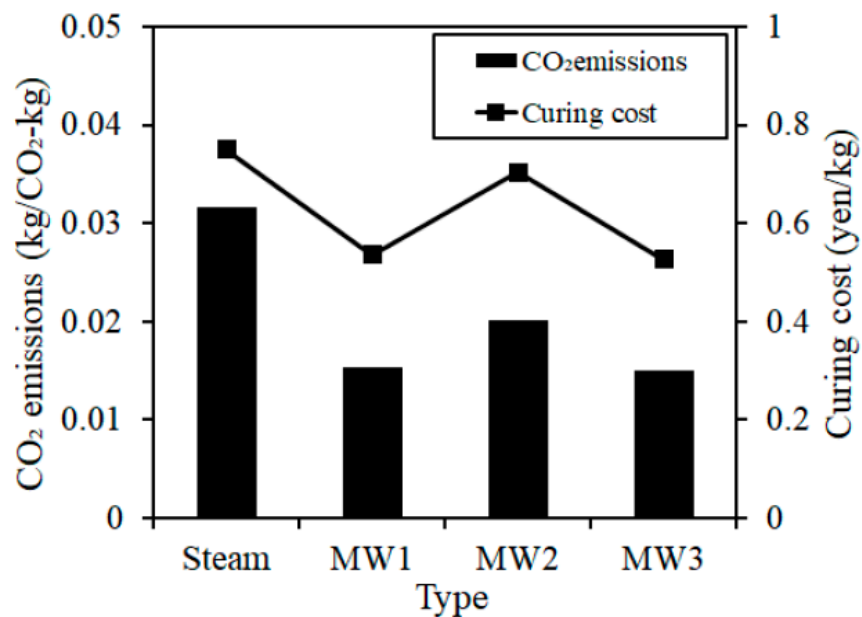


Figure 13. Comparison of traditional steam curing with MW-T (open access status) [135].

The effect of MW-T on the production of concrete and mortar was studied by Leung and Pheeraphan [136]. They developed an effective process for concrete ($w/c = 0.33$) that produced unexpected results in terms of 4.5 h f_c reaching 35.4 MPa and the 7-day strength being 57.0 MPa (in the case of $w/c = 0.40$, the strength reached 29.5 MPa at 4.5 h and 48.0 MPa at 7 days).

Applying a microwave could remove free water while the slurry is still in its plastic state, reducing the water–cement ratio of the mixture, which can make up for the strength loss during the heating process [136–138]. Microwave pre-curing may also reduce the porosity of mortar and increase its f_c . MW-T can potentially be used in various building processes, such as concrete pre-casting and repair, to obtain extraordinarily high early strengths while conserving much energy.

The number of CH crystals, the size of the CH face (001), and the preferred orientation of CH all decreased as a consequence of microwave curing, as found by Gao et al. [139]. Microwave curing developed a granular C-S-H gel with a high Ca/Si atomic ratio (nearly 3.5) in hydrated PC. Microwave curing and steam curing increased the polymerization of C-S-H gel compared to conventional curing. In addition, MW-T curing for 45 min resulted in a greater hydration of PC than steam curing at 80 °C for 4 h or conventional curing for 12 h. Microwave and steam curing hastened the hydration of C_3S and C_2S , respectively. Compared to steam curing and normal curing, microwave curing substantially expedited cement hydration while also increasing the content of medium capillary pores in the hardened paste.

In order to determine microwave curing's impact on the development of f_c in mortar made with the cement–GGBFS evolution of temperature and the water-to-binder ratio, as well as the composite binder and its underlying process during curing, the hydration products and the microstructure of the composite system were studied [140]. The findings demonstrate that the highest microwave-curing temperature is slightly lower, and the final water-to-binder ratios are slightly lower as GGBFS content increases. Due to its long reaction time with water, GGBS is referred to as a latent hydraulic substance [141]. The ST test tangentially demonstrates the microwave's non-thermal action on composite systems. Steam curing is less effective than microwaves at carbonating composite binders. Together with the acceleration of hydration at early ages, a key element in improving the f_c of composed with the cement-mortar–GGBFS composite binder is the reduction in detrimental pores. The microwave's drying effect can greatly reduce mortar's porosity by lowering the water-to-binder ratio. Moreover, the hydration of composite systems can be accelerated by the thermal and non-thermal effects of microwaves, and microwave curing can enhance and homogenize the pore structure of mortar.

The characteristics of magnesium phosphate cement were affected by using a microwave oven in the calcination of MgO by Ribeiro et al. [142]. Microwave radiation preferentially links particles with larger dielectric loss during this calcination process, which differs from conventional calcination. If the dopant has a low dielectric loss, a doped powder that can be successfully and quickly calcined in a normal oven may not necessarily show the same results when calcined in a microwave. The microwave calcination was effective in the process of decreasing the MgO surface area and, as a result, in increasing the cement's setting time. This allowed for greater control of the reactions during the setting, producing specimens with a low open porosity and high mechanical strength, but it also increased the tendency to exudate certain volumes of water.

To create conductive gratings using a carbon nanotube (CNT), Wang et al. [143] combined a cement composite with aluminum silicate ceramic fiberboard as the dielectric layer, resulting in a unique and practical cementitious metastructure. The microwave absorption of prepared specimens was greatly enhanced by an absorbing metastructure based on CNT gratings. The metastructure (24 mm) periodicity gratings demonstrated multi-band absorption capabilities with five peaks less than -20 dB. The metastructure (14/24 filling fraction gratings) demonstrated excellent broadband absorption performance with a reflectance peak of -38.7 dB and bandwidth of -15 dB at 13.0 GHz.

The temperature distribution, structural compactness, and strength development of the Cemented Tailings Backfill (CTB) can all be significantly impacted by MW-T, according to Sun et al. [144]. Underground mined-out sections are filled with CTB, typically made by combining tailings, a binder, and water. To ensure safe and effective mining production, the CTB should soon reach sufficient strength when buried. With varied curing ages, solid contents, and binder-to-tailings ratios when the same MW-T is applied, the CTB exhibits different thermal and mechanical behavior. According to the current investigation, the microwave approach may increase the stability and durability of the prepared CTB structures. The timing of the MW-T implementation is also crucial; therefore, the interval between the implantation of the CTB and microwave heating is considered. In the CTB at an early age, a shorter delay time is linked to greater mechanical performance. At a curing age of 7 days, microwave heating (for 7 min) with a 0 h delay period can also boost the CTB's strength [145]. To ensure safe and effective mining, the CTB strength and gain rate should also be ensured. The CTB heated with MW-T is described in work by Sun et al. [146] as using a coupled electromagnetic heat transfer model. This suggested model considers the processes of heat conduction and convection, as well as pertinent temperature variation. Energy is converted from electrical to electromagnetic and then thermal. The practical application of the microwave approach to the CTB technology can thus advance, thanks in part to the findings of this investigation. This work is anticipated to contribute to the practical implementation of microwave technology in mine backfill operations. A summary of the major effects of microwave treatment MW-T on concrete curing effectiveness is given in Table 3.

Table 3. Summary of the effects of microwave treatment (MW-T) on concrete curing effectiveness.

Aggregates (F-Fine, C-Coarse)	SCMs/Replacement Levels (%)	Main Findings	Treatment Refs.
F: quartz sand	Limestone powder/(21.1) SF/(16.7)	- In comparison to the reference specimens, the f_c displays increments of 30 MPa, 53 MPa, 74 MPa, and 89 MPa with microwave exposure times of 60 s, 120 s, 180 s, and 240 s at the age of 8 h. Here, microwave pre-curing for 240 s results in the highest f_c of 105 MPa.	MW-T [137]
F: quartz sand	SF, FA	- Due to MW-T curing, it is possible to generate materials with very high early strength up to 420 MPa after just one day and a total microwave-curing time of two hours. - The hydration and pozzolanic reactions were accelerated at the same time by MW-T curing and the application of very reactive pozzolanic additives.	MW-T [138]
-	GGBFS/(15, 30, 45)	- The carbonation of composite binders can be promoted more quickly with MW-T curing than with steam curing. Along with the acceleration of hydration at early ages, an important factor in improving the f_c of composed with cement mortar-GGBFS composite binder is the decrease in the number of harmful pores.	MW-T [140]
F: quartz sand	SF/(25.9)	- Aluminosilicate chain length for C-S-H phase with more branches and cross-linking are created during hydration at a high output energy of MW-T curing.	MW-T [147]
-	Graphene-oxide (GO) doping/(0.05, 0.1, 0.5)	- The synergetic effect of combining GO-doping and MW-T curing resulted in the maximum f_c (32.4 MPa), which is about 126.6% more than what would have been possible without GO-doping and MW-T curing.	MW-T [148]
-	FA/(50)	- In contrast to the very low early-age strength of the cement-FA blended paste under air curing (11 MPa at 1 day), cement-FA blended paste gained 51.5 MPa under MW-T curing for 5.29 h. - Low energy low-carbon concrete can be produced via MW-T curing.	MW-T [149]
F: river sand	Coal gangue/(30)	- The optimal MW-T curing temperature range was 600 °C–700 °C, and microwaves can stimulate the activity of coal gangue powder. - The high temperature of MW-T curing also led coal gangue powder to dissolve, which resulted in the particles becoming fine and moist.	MW-T [150]
F: nonreactive sand	Bamboo culms/(1, 1.5)	- Alkaline treatment with MW-T increased the ductility and toughness of prepared composites.	MW-T [151]

“-” denotes no aggregate present, i.e., cement paste.

4.2. MW-T for Recycled Aggregates

The MW-T of concrete has the potential to provide a brand-new, extremely effective, and energy-efficient method of recycling aggregates. Microwave-assisted aggregate recovery from saturated concrete can be more effective and efficient, with significantly less performance loss [152]. Increasing the water content of crushed concrete could produce better aggregate recycling outcomes for industrial applications. Better recycling results can be obtained by watering or purling on crushed concrete first, then moving it to microwave heating equipment to begin the separating process (Figure 14). In comparison to the traditional mechanical separation procedure or the microwave heating method, the approach was more practical and convenient for the environment.

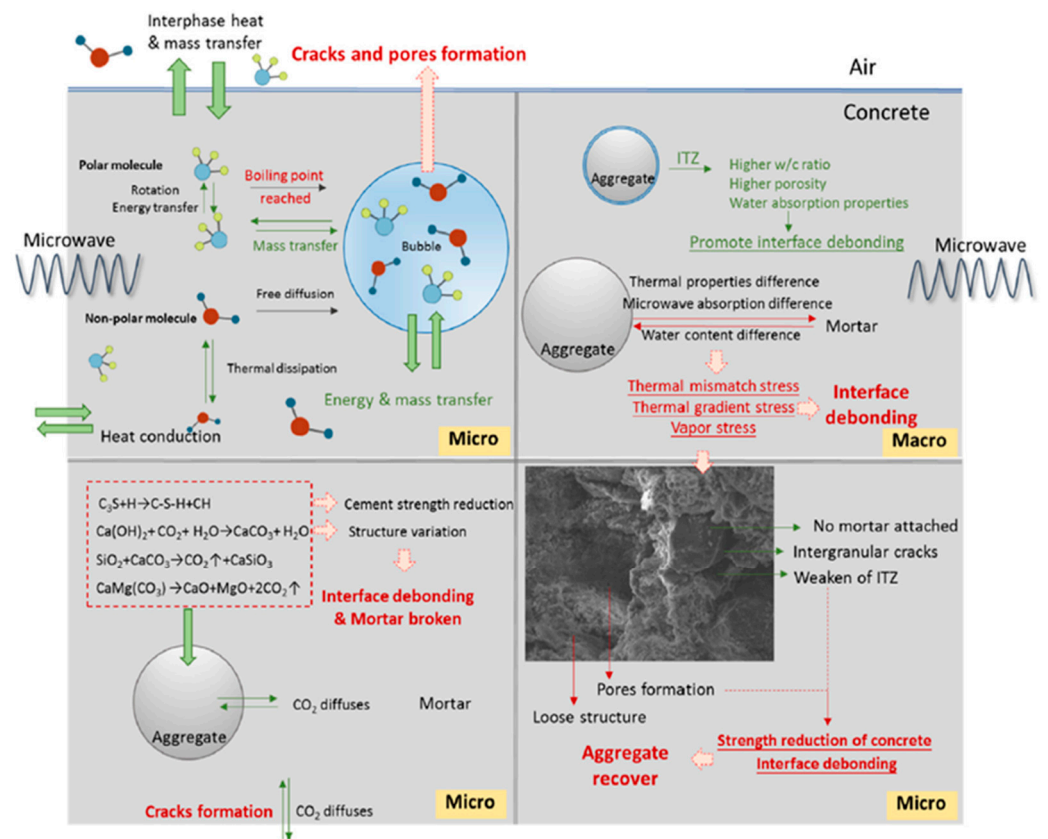


Figure 14. Diagram of concrete’s microwave heating system (with permission from [103]).

For concrete, temperature-gradient-induced cracks began in the specimen’s middle region and spread to the specimen surface, and the beginning and growth of cracks induced by temperature gradients were dependent on the temperature difference [103]. Due to the differences in properties between aggregate and mortar, cracks were formed along the interface between the mortar matrix and the aggregates. Based on the outcomes of the experiment, higher microwave input does not result in a larger temperature difference between mortar and aggregates; however, it results in more severe interface damage (Figure 14). The size and strength of the concrete will also impact the outcome of the aggregate recovery. The microwave heating cavity’s feature can be more suitable for concrete with particular proportions. It still needs to be clarified how to choose the most efficient heating parameters when other concrete and aggregate qualities are considered. The proper heating conditions are required to achieve a better separation effect while minimizing aggregate property damage.

The effectiveness of MW-T for the surface modification of recycled aggregates was studied by Choi et al. [153]. The surface-modified coarse aggregate (SMCA) and the aggregate interface were heated differently to over 100 °C thanks to MW-T (Figure 15),

which enables selective heating. Based on this finding, it was revealed that microwave heating successfully heated the iron oxide blended with the SMCA. The temperature of SMCA concrete containing iron oxide, a dielectric substance, increased higher than it did for original coarse aggregate (OCA) concrete when heated with microwaves. The concrete started to microcrack, particularly when it was heated for longer than 180 s, and the highest temperature was over 400 °C.

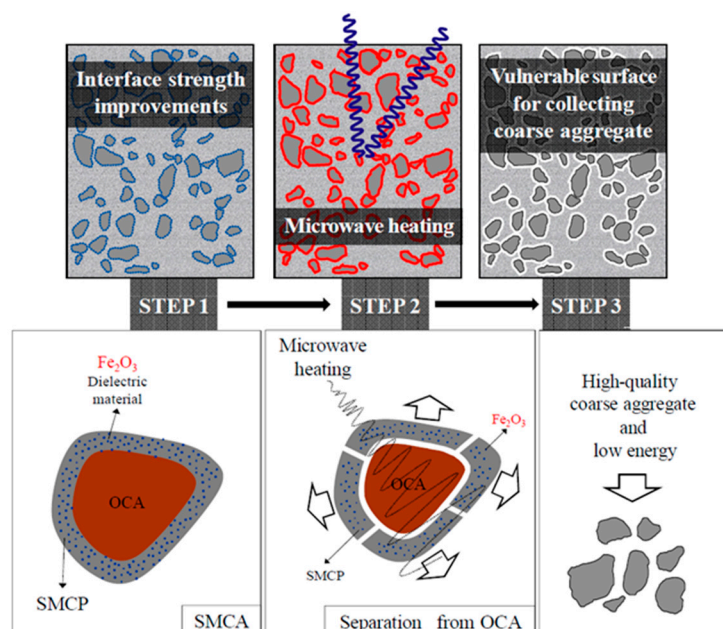


Figure 15. Microwave modification and recovery of recycled aggregates (open access status) [153].

This was accompanied by an increase in void size distribution brought on by a dehydration reaction of the hydrates. This, in turn, led to the $\text{Ca}(\text{OH})_2$ and CaCO_3 decomposing, weakening and decreasing the strength of the cement paste. The recycled coarse aggregate (RCA) that was recovered with microwave heating for 180 s had around 2–3% paste and fine aggregate. The recovered RCA was extremely comparable to the recovered RCA from OCA concrete, suggesting the potential for recovering high-quality RCA. It has been discovered that microwave heating weakens the binder that includes a dielectric substance, enabling the effective recovery of RCA.

5. Concluding Remarks and Future Perspectives

A rising range of cementitious materials and concrete are being produced at the laboratory scale using non-ionizing radiation. Many of these materials can now be created by employing microwaves, sonication, and magnetic fields, as well as by moving beyond the restrictions of standard preparation procedures, as illustrated by the recent selection of innovative constituents and concrete mixture formulations. The following features of cementitious mixtures are affected by power ultrasound treatment US-T and Magnetic Field Treatment (MF-T):

- Particle dispersion in the mixes,
- Rheological properties of the mixes,
- The setting time and the heat of hydration of cement,
- The early and the late strength,
- The capillary porosity,
- Concrete durability indicators.

On the other hand, the microwave treatment MW-T is found to be beneficial for recycled aggregate preparation and the effective curing of concrete. However, at present, the applicability of these techniques for low-clinker cement materials has not been demon-

strated convincingly. In particular, the effects of increased temperature during US-T have not been clearly distinguished from the actual effects of power during US-T. The semi-industrial trials are also lacking.

The beneficiation of constituents and their more effective dispersion in concrete mixtures still need a better explanation. From the standpoint of material science, further research is needed to identify the specific effects of these novel preparation methods on the fundamental physicochemical processes determining the properties of early-age concrete. Rahimi-Aghdam et al.'s model [56] identified the principal phenomena that control the early hydration kinetics of cement, including the dissolution of clinker phases, the initiation of the precipitation of solid products either homogeneously in solution or heterogeneously on a solid surface, the diffusion of solution components through the pore volume of cement paste, and the growth of hydration products. The identification of the diffusive properties of low-clinker cementitious materials, such as CEM II/C-M [6], developed utilizing innovative preparation procedures, will be intriguing. It is still important to create applicable, thorough hydration models for low-clinker cement types with high slag and limestone content. Then, the model's parameters could be discovered. Therefore, an empirical study can currently be undertaken to determine the benefits of the suggested material-preparation techniques for low-carbon-footprint materials. But this might also involve more advanced research on combining these techniques. It is anticipated that new improvements in advanced material preparation, which will eventually replace simple constituent mixing, will have a considerable impact on the creation of highly engineered concrete mixtures for the green construction industry.

Author Contributions: Conceptualization, P.L.; writing—original draft preparation, P.L.; data curation, P.L.; formal analysis, P.L.; investigation, P.L.; methodology, P.L.; validation, P.L.; visualization, P.L.; writing—review and editing, P.L. and M.A.G.; supervision, M.A.G. All authors have read and agreed to the published version of the manuscript.

Funding: This research received no external funding.

Institutional Review Board Statement: Not applicable.

Informed Consent Statement: Not applicable.

Data Availability Statement: Data are contained within the article.

Conflicts of Interest: The authors declare no conflict of interest.

Abbreviations

CTB	Cemented Tailings Backfill
DSF	Densified Silica Fume
EN-Al	Egyptian nano-Al ₂ O ₃
FA	Fly Ash
fc	Compressive Strength
fst	Splitting Tensile Strength
GWD	Granite Waste Dust
GO	Graphene-oxide
GGBFS	Ground Granulated Blast Furnace Slag
HGM	Hollow Glass Microspheres
MF-T	Magnetic Field Treatment
M-Water	Magnetized Water
MWD	Marble waste dust
MW-T	Microwave Treatment
NSF	Nano-silica Fume
NDSF	Non-Densified Silica Fume
OCA	Original coarse aggregate
PC	Portland Cement

PFA	Pulverized Fuel Ash
RCA	Recycled Coarse Aggregate
SF	Silica Fume
SSF	Sonicated Silica Fume
S-CC	Self-Compacting Concrete
S-CLC	Self-Compacting Lightweight Concrete
SCMs	Supplementary Cementitious Materials
SMCA	Surface-Modified Coarse Aggregate
US-T	Ultrasound Treatment
UCFA	Untreated Coal Fine Aggregate
VA	Volcanic Ash
σ	Surface Tension Coefficient

References

- Gawlicki, M. Belite in Cements with Low Emission of CO₂ during Clinker Formation. *Cem. Wapno Beton.* **2020**, *25*, 348–357. [\[CrossRef\]](#)
- Palm, S.; Müller, C.; Proske, T.; Rezvani, M.; Graubner, C.-A. Concrete Application of Clinker-Efficient Cements. *Adv. Cem. Res.* **2019**, *31*, 225–234. [\[CrossRef\]](#)
- Müller, C.; Severins, K.; Spanka, G. Crushed sand as a main cement constituent-guidelines for future use in cement and concrete. *Cem. Int.* **2019**, *17*, 38–61.
- Zajac, M.; Skocek, J.; Durdzinski, P.; Bullerjahn, F.; Skibsted, J.; Ben Haha, M. Effect of Carbonated Cement Paste on Composite Cement Hydration and Performance. *Cem. Concr. Res.* **2020**, *134*, 106090. [\[CrossRef\]](#)
- Palm, S.; Proske, T.; Rezvani, M.; Hainer, S.; Müller, C.; Graubner, C.A. Cements with a High Limestone Content—Mechanical Properties, Durability and Ecological Characteristics of the Concrete. *Constr. Build. Mater.* **2016**, *119*, 308–318. [\[CrossRef\]](#)
- BS EN 197-5; Cement—Part 5: Portland-Composite Cement CEM II/C-M and Composite Cement CEM VI. British Standards Institution: Loughborough, UK, 2021. [\[CrossRef\]](#)
- Gu, Y.; Bary, B.; Machner, A.; De Weerd, K.; Bolte, G.; Ben Haha, M. Multi-Scale Strategy to Estimate the Mechanical and Diffusive Properties of Cementitious Materials Prepared with CEM II/C-M. *Cem. Concr. Compos.* **2022**, *131*, 104537. [\[CrossRef\]](#)
- Müller, C.; Palm, S.; Hermerschmidt, W. Durability properties of concretes using CEM II/C-M (S-LL) and CEM II/B-LL cements. *Cem. Int.* **2020**, *18*, 52–62.
- Proske, T.; Rezvani, M.; Palm, S.; Müller, C.; Graubner, C.A. Concretes Made of Efficient Multi-Composite Cements with Slag and Limestone. *Cem. Concr. Compos.* **2018**, *89*, 107–119. [\[CrossRef\]](#)
- Chen, H.; Hou, P.; Zhou, X.; Black, L.; Adu-Amankwah, S.; Feng, P.; Cui, N.; Glinicki, M.A.; Cai, Y.; Zhang, S.; et al. Toward Performance Improvement of Supersulfated Cement by Nano Silica: Asynchronous Regulation on the Hydration Kinetics of Silicate and Aluminate. *Cem. Concr. Res.* **2023**, *167*, 107117. [\[CrossRef\]](#)
- Chen, L.; Su, R.K.L. Experimental and Numerical Investigations on Macrocell Corrosion of Partially Carbonated Reinforced Concrete with Supplementary Cementitious Materials. *Cem. Concr. Compos.* **2023**, *135*, 104827. [\[CrossRef\]](#)
- von Greve-Dierfeld, S.; Lothenbach, B.; Vollpracht, A.; Wu, B.; Huet, B.; Andrade, C.; Medina, C.; Thiel, C.; Gruyaert, E.; Vanoutrive, H.; et al. Understanding the Carbonation of Concrete with Supplementary Cementitious Materials: A Critical Review by RILEM TC 281-CCC. *Mater. Struct.* **2020**, *53*, 136. [\[CrossRef\]](#)
- Juenger, M.C.G.; Siddique, R. Recent Advances in Understanding the Role of Supplementary Cementitious Materials in Concrete. *Cem. Concr. Res.* **2015**, *78*, 71–80. [\[CrossRef\]](#)
- Lothenbach, B.; Scrivener, K.; Hooton, R.D. Supplementary Cementitious Materials. *Cem. Concr. Res.* **2011**, *41*, 1244–1256. [\[CrossRef\]](#)
- Suraneni, P.; Hajibabae, A.; Ramanathan, S.; Wang, Y.; Weiss, J. New Insights from Reactivity Testing of Supplementary Cementitious Materials. *Cem. Concr. Compos.* **2019**, *103*, 331–338. [\[CrossRef\]](#)
- Shah, I.H.; Miller, S.A.; Jiang, D.; Myers, R.J. Cement Substitution with Secondary Materials Can Reduce Annual Global CO₂ Emissions by up to 1.3 Gigatons. *Nat. Commun.* **2022**, *13*, 5758. [\[CrossRef\]](#) [\[PubMed\]](#)
- Saleh Ahari, R.; Kemal Erdem, T.; Ramyar, K. Effect of Various Supplementary Cementitious Materials on Rheological Properties of Self-Consolidating Concrete. *Constr. Build. Mater.* **2015**, *75*, 89–98. [\[CrossRef\]](#)
- Escalante-García, J.I.; Sharp, J.H. The Microstructure and Mechanical Properties of Blended Cements Hydrated at Various Temperatures. *Cem. Concr. Res.* **2001**, *31*, 695–702. [\[CrossRef\]](#)
- Ozturk, M.; Karaaslan, M.; Akgol, O.; Sevim, U.K. Mechanical and Electromagnetic Performance of Cement Based Composites Containing Different Replacement Levels of Ground Granulated Blast Furnace Slag, Fly Ash, Silica Fume and Rice Husk Ash. *Cem. Concr. Res.* **2020**, *136*, 106177. [\[CrossRef\]](#)
- Harbec, D.; Tagnit-Hamou, A.; Gitzhofer, F. Waste-Glass Fume Synthesized Using Plasma Spheroidization Technology: Reactivity in Cement Pastes and Mortars. *Constr. Build. Mater.* **2016**, *107*, 272–286. [\[CrossRef\]](#)

21. Dilissen, N.; Vleugels, J.; Vermeiren, J.; García-Baños, B.; Marín, J.R.S.; Catalá-Civera, J.M. Temperature Dependency of the Dielectric Properties of Hydrated and Ordinary Portland Cement and Their Constituent Phases at 2.45 GHz up to 1100 °C. *Cem. Concr. Res* **2023**, *165*, 107067. [[CrossRef](#)]
22. Vrdoljak, I.; Varevac, D.; Miličević, I.; Čolak, S. Concrete-Based Composites with the Potential for Effective Protection against Electromagnetic Radiation: A Literature Review. *Constr. Build. Mater.* **2022**, *326*, 126919. [[CrossRef](#)]
23. Sáez del Bosque, I.F.; Medina, J.M.; Frías, M.; Sánchez de Rojas, M.I.; Medina, C. Use of Biomass-Fired Power Plant Bottom Ash as an Addition in New Blended Cements: Effect on the Structure of the C-S-H Gel Formed during Hydration. *Constr. Build. Mater.* **2019**, *228*, 117081. [[CrossRef](#)]
24. Guo, H.; Wang, Z.; An, D.; Huo, J. Collaborative Design of Cement-Based Composites Incorporated with Cooper Slag in Considerations of Engineering Properties and Microwave-Absorbing Characters. *J. Clean. Prod.* **2021**, *283*, 124614. [[CrossRef](#)]
25. Ghafari, E.; Ghahari, S.A.; Costa, H.; Júlio, E.; Portugal, A.; Durães, L. Effect of Supplementary Cementitious Materials on Autogenous Shrinkage of Ultra-High Performance Concrete. *Constr. Build. Mater.* **2016**, *127*, 43–48. [[CrossRef](#)]
26. Glinicki, M.A.; Dąbrowski, M.; Antolik, A.; Dziedzic, K.; Sikorin, S.; Fateev, V.; Povolansky, E. Gamma Irradiation Sensitivity of Early Hardening Cement Mortar. *Cem. Concr. Compos.* **2022**, *126*, 104327. [[CrossRef](#)]
27. Dąbrowski, M.; Glinicki, M.A.; Dziedzic, K.; Józwiak-Niedźwiedzka, D.; Sikorin, S.; Fateev, V.S.; Povalansky, E.I. Early Age Hardening of Concrete with Heavy Aggregate in Gamma Radiation Source—Impact on the Modulus of Elasticity and Microstructural Features. *J. Adv. Concr. Technol.* **2021**, *19*, 555–570. [[CrossRef](#)]
28. De Schutter, G.; Lesage, K. Active Control of Properties of Concrete: A (p)Review. *Mater. Struct.* **2018**, *51*, 123. [[CrossRef](#)]
29. Lott, M.; Remillieux, M.C.; Garnier, V.; Ulrich, T.J.; Le Bas, P.Y.; Deraemaeker, A.; Dumoulin, C.; Payan, C. Fracture Processes Imaging in Concrete Using Nonlinear Ultrasound. *NDT E Int.* **2021**, *120*, 102432. [[CrossRef](#)]
30. Ganjian, E.; Ehsani, A.; Mason, T.J.; Tyrer, M. Application of Power Ultrasound to Cementitious Materials: Advances, Issues and Perspectives. *Mater. Des.* **2018**, *160*, 503–513. [[CrossRef](#)]
31. Ehsani, A.; Ganjian, E.; Mason, T.J.; Tyrer, M.; Bateman, M. Insights into the Positive Effects of Power Ultrasound on the Pore Structure of Portland Cement Pastes. *Cem. Concr. Compos.* **2022**, *125*, 104302. [[CrossRef](#)]
32. Colmenares, J.C. Sonication-Induced Pathways in the Synthesis of Light-Active Catalysts for Photocatalytic Oxidation of Organic Contaminants. *ChemSusChem* **2014**, *7*, 1512–1527. [[CrossRef](#)] [[PubMed](#)]
33. Hangxun, X.; Zeiger, B.W.; Suslick, K.S. Sonochemical Synthesis of Nanomaterials. *Chem. Soc. Rev.* **2013**, *42*, 2555–2567. [[CrossRef](#)]
34. Lisowski, P.; Colmenares, J.C.; Mašek, O.; Lisowski, W.; Lisovytskiy, D.; Grzonka, J.; Kurzydłowski, K. Design and Fabrication of TiO₂/Lignocellulosic Carbon Materials: Relevance of Low-Temperature Sonocrystallization to Photocatalysts Performance. *ChemCatChem* **2018**, *10*, 3469–3480. [[CrossRef](#)]
35. Lisowski, P.; Colmenares, J.C.; Mašek, O.; Lisowski, W.; Lisovytskiy, D.; Kamińska, A.; Łomot, D. Dual Functionality of TiO₂/Biochar Hybrid Materials: Photocatalytic Phenol Degradation in the Liquid Phase and Selective Oxidation of Methanol in the Gas Phase. *ACS Sustain. Chem. Eng.* **2017**, *5*, 6274–6287. [[CrossRef](#)]
36. Colmenares, J.C.; Varma, R.S.; Lisowski, P. Sustainable Hybrid Photocatalysts: Titania Immobilized on Carbon Materials Derived from Renewable and Biodegradable Resources. *Green. Chem.* **2016**, *18*, 5736–5750. [[CrossRef](#)] [[PubMed](#)]
37. Chatel, G.; Novikova, L.; Petit, S. How Efficiently Combine Sonochemistry and Clay Science? *Appl. Clay Sci.* **2016**, *119*, 193–201. [[CrossRef](#)]
38. Sander, J.R.G.; Zeiger, B.W.; Suslick, K.S. Sonocrystallization and Sonofragmentation. *Ultrason. Sonochem* **2014**, *21*, 1908–1915. [[CrossRef](#)]
39. Luque de Castro, M.D.; Priego-Capote, F. Ultrasound-Assisted Crystallization (Sonocrystallization). *Ultrason. Sonochem* **2007**, *14*, 717–724. [[CrossRef](#)]
40. Tomczak, K.; Jakubowski, J.; Kotwica, Ł. Self-Sealing Process Evaluation Method Using Ultrasound Technique in Cement Composites with Mineral Additives. *Materials* **2020**, *13*, 3336. [[CrossRef](#)]
41. Haach, V.G.; Juliani, L.M. Possibilities of Using Ultrasound for the Technological Control of Concrete of Hollow-Core Slabs. *Constr. Build. Mater.* **2017**, *133*, 409–415. [[CrossRef](#)]
42. Ospitia, N.; Jaramani, R.; Remy, O.; Aggelis, D.G. Determination of Concrete Formwork Removal Time Based on Ultrasound Reflection. *Appl. Sci.* **2022**, *12*, 1221. [[CrossRef](#)]
43. Ham, S.; Popovics, J.S. Application of Contactless Ultrasound toward Automated Inspection of Concrete Structures. *Autom. Constr.* **2015**, *58*, 155–164. [[CrossRef](#)]
44. Kim, G.; Kim, J.Y.; Kurtis, K.E.; Jacobs, L.J. Drying Shrinkage in Concrete Assessed by Nonlinear Ultrasound. *Cem. Concr. Res.* **2017**, *92*, 16–20. [[CrossRef](#)]
45. Kim, G.; Kurtis, K.E. Early-Stage Assessment of Drying Shrinkage in Portland Limestone Cement Concrete Using Nonlinear Ultrasound. *Constr. Build. Mater.* **2022**, *342*, 128099. [[CrossRef](#)]
46. Quiviger, A.; Payan, C.; Chaix, J.F.; Garnier, V.; Salin, J. Effect of the Presence and Size of a Real Macro-Crack on Diffuse Ultrasound in Concrete. *NDT E Int.* **2012**, *45*, 128–132. [[CrossRef](#)]
47. Quiviger, A.; Girard, A.; Payan, C.; Chaix, J.F.; Garnier, V.; Salin, J. Influence of the Depth and Morphology of Real Cracks on Diffuse Ultrasound in Concrete: A Simulation Study. *NDT E Int.* **2013**, *60*, 11–16. [[CrossRef](#)]
48. Liu, X.; Sun, D.; Liu, D.; Meng, K.; Ni, C.; Shao, Z.; Sun, L. Simulation of Ultrasonic Propagation in Porous Cellular Concrete Materials. *Constr. Build. Mater.* **2021**, *285*, 122852. [[CrossRef](#)]

49. Guan, X.; Chen, J.; Qiu, J.; Gao, Y.; Gao, J. Damage Evaluation Method Based on Ultrasound Technique for Gangue Concrete under Freezing-Thawing Cycles. *Constr. Build. Mater.* **2020**, *246*, 118437. [[CrossRef](#)]
50. Abo-Qudais, S.A. Effect of Concrete Mixing Parameters on Propagation of Ultrasonic Waves. *Constr. Build. Mater.* **2005**, *19*, 257–263. [[CrossRef](#)]
51. Dong, W.; Wu, Z.; Zhou, X.; Tan, Y. Experimental Studies on Void Detection in Concrete-Filled Steel Tubes Using Ultrasound. *Constr. Build. Mater.* **2016**, *128*, 154–162. [[CrossRef](#)]
52. Salvador, R.P.; Cavalaro, S.H.P.; Segura, I.; Hernández, M.G.; Ranz, J.; Figueiredo, A.D. de Relation between Ultrasound Measurements and Phase Evolution in Accelerated Cementitious Matrices. *Mater. Des.* **2017**, *113*, 341–352. [[CrossRef](#)]
53. Askarnejad, A.; Pourkhorshidi, A.R.; Parhizkar, T. Evaluation the Pozzolanic Reactivity of Sonochemically Fabricated Nano Natural Pozzolan. *Ultrason. Sonochem.* **2012**, *19*, 119–124. [[CrossRef](#)]
54. Alizadeh, R.; Raki, L.; Makar, J.M.; Beaudoin, J.J.; Moudrakovski, I. Hydration of Tricalcium Silicate in the Presence of Synthetic Calcium–Silicate–Hydrate. *J. Mater. Chem.* **2009**, *19*, 7937–7946. [[CrossRef](#)]
55. Singh, L.P.; Bhattacharyya, S.K.; Shah, S.P.; Mishra, G.; Sharma, U. Studies on Early Stage Hydration of Tricalcium Silicate Incorporating Silica Nanoparticles: Part II. *Constr. Build. Mater.* **2016**, *102*, 943–949. [[CrossRef](#)]
56. Nishida, I. Precipitation of Calcium Carbonate by Ultrasonic Irradiation. *Ultrason. Sonochem.* **2004**, *11*, 423–428. [[CrossRef](#)] [[PubMed](#)]
57. Diamond, S.; Sahu, S.; Thaulow, N. Reaction Products of Densified Silica Fume Agglomerates in Concrete. *Cem. Concr. Res.* **2004**, *34*, 1625–1632. [[CrossRef](#)]
58. Rahimi-Aghdam, S.; Bažant, Z.P.; Abdolhosseini Qomi, M.J. Cement Hydration from Hours to Centuries Controlled by Diffusion through Barrier Shells of C-S-H. *J. Mech. Phys. Solids* **2017**, *99*, 211–224. [[CrossRef](#)]
59. Kumar, R.; Bhattacharjee, B. Porosity, Pore Size Distribution and in Situ Strength of Concrete. *Cem. Concr. Res.* **2003**, *33*, 155–164. [[CrossRef](#)]
60. Scrivener, K.L.; Nonat, A. Hydration of Cementitious Materials, Present and Future. *Cem. Concr. Res.* **2011**, *41*, 651–665. [[CrossRef](#)]
61. Vaitkevičius, V.; Šerelis, E.; Kerševičius, V. Effect of Ultra-Sonic Activation on Early Hydration Process in 3D Concrete Printing Technology. *Constr. Build. Mater.* **2018**, *169*, 354–363. [[CrossRef](#)]
62. Rodríguez, E.D.; Bernal, S.A.; Provis, J.L.; Payá, J.; Monzó, J.M.; Borrachero, M.V. Structure of Portland Cement Pastes Blended with Sonicated Silica Fume. *J. Mater. Civ. Eng.* **2012**, *24*, 1295–1304. [[CrossRef](#)]
63. Hashem, M.M.; Serag, M.I.; El-Kady, H.; El-Feky, M. Increasing the reactivity of silica fume particles using indirect sonication: Effect of process parameters. *Int. J. Mod. Trends Eng. Res.* **2015**, *2*, 2349.
64. Ni, C.; Wu, Q.; Yu, Z.; Shen, X. Hydration of Portland Cement Paste Mixed with Densified Silica Fume: From the Point of View of Fineness. *Constr. Build. Mater.* **2021**, *272*, 121906. [[CrossRef](#)]
65. Bajja, Z.; Dridi, W.; Darquennes, A.; Bennacer, R.; Le Bescop, P. Effect of Aggregates on the Diffusion Properties and Microstructure of Cement with Slurried Silica Fume Based Materials. *Cem. Concr. Compos.* **2016**, *70*, 86–97. [[CrossRef](#)]
66. Wang, X.; Huang, J.; Dai, S.; Ma, B.; Tan, H.; Jiang, Q. Effect of Silica Fume Particle Dispersion and Distribution on the Performance of Cementitious Materials: A Theoretical Analysis of Optimal Sonication Treatment Time. *Constr. Build. Mater.* **2019**, *212*, 549–560. [[CrossRef](#)]
67. Geng, Z.; Tang, S.; Wang, Y.; He, Z.; Wu, K. The stress relaxation properties of calcium silicate hydrate: A molecular dynamics study. *J. Zhejiang Univ. Sci. A* **2023**, *1*–22. [[CrossRef](#)]
68. Martínez-Velandia, D.; Payá, J.; Monzó, J.; Borrachero, M.V. Effect of Sonication on the Reactivity of Silica Fume in Portland Cement Mortars. *Adv. Cement Res.* **2015**, *23*, 23–31. [[CrossRef](#)]
69. Rodríguez, E.D.; Soriano, L.; Payá, J.; Borrachero, M.V.; Monzó, J.M. Increase of the Reactivity of Densified Silica Fume by Sonication Treatment. *Ultrason. Sonochem.* **2012**, *19*, 1099–1107. [[CrossRef](#)]
70. Sharobim, K.G.; Mohammedin, H.; Hanna, N.F.; El-Feky, M.S.; Khattab, E.; El-Tair, A.M. Optimizing sonication time and solid to liquid ratio of nano-silica in high strength concrete. *Int. J. Sci. Eng. Res.* **2017**, *8*, 687–693.
71. Martínez-Velandia, D.; Payá, J.; Monzó, J.; Borrachero, M.V. Granulometric Activation of Densified Silica Fume (CSF) by Sonication. *Adv. Cem. Res.* **2015**, *20*, 129–135. [[CrossRef](#)]
72. Ramalingam, M.; Narayanan, K.; Masilamani, A.; Kathirvel, P.; Murali, G.; Vatin, N.I. Influence of Magnetic Water on Concrete Properties with Different Magnetic Field Exposure Times. *Materials* **2022**, *15*, 4291. [[CrossRef](#)]
73. Ibrahim, E.M.; Abbas, Z.K. Effect of Magnetic Water on Strength Properties of Concrete. *IOP Conf. Ser. Mater. Sci. Eng.* **2021**, *1067*, 012002. [[CrossRef](#)]
74. Ghorbani, S.; Sharifi, S.; de Brito, J.; Ghorbani, S.; Jalayer, M.A.; Tavakkolizadeh, M. Using Statistical Analysis and Laboratory Testing to Evaluate the Effect of Magnetized Water on the Stability of Foaming Agents and Foam Concrete. *Constr. Build. Mater.* **2019**, *207*, 28–40. [[CrossRef](#)]
75. Mohammadnezhad, A.; Azizi, S.; Sousanabadi Farahani, H.; Tashan, J.; Habibnejad Korayem, A. Understanding the Magnetizing Process of Water and Its Effects on Cementitious Materials: A Critical Review. *Constr. Build. Mater.* **2022**, *356*, 129076. [[CrossRef](#)]
76. Ghazy, M.F.; Abd Elaty, M.A.A.; Daboun, O. Fracture Properties of Self-Compacting Fiber-Reinforced Concrete. *Chall. J. Concr. Res. Lett.* **2020**, *11*, 112. [[CrossRef](#)]
77. Liu, J.; Cao, Y. Experimental Study on the Surface Tension of Magnetized Water. *Int. Commun. Heat. Mass. Transf.* **2021**, *121*, 105091. [[CrossRef](#)]

78. Iino, M.; Fujimura, Y. Surface Tension of Heavy Water under High Magnetic Fields. *Appl. Phys. Lett.* **2009**, *94*, 261902. [CrossRef]
79. Cai, R.; Yang, H.; He, J.; Zhu, W. The Effects of Magnetic Fields on Water Molecular Hydrogen Bonds. *J. Mol. Struct.* **2009**, *938*, 15–19. [CrossRef]
80. Abdel-Magid, T.I.M.; Hamdan, R.M.; Abdelgader, A.A.B.; Omer, M.E.A.; Ahmed, N.M.R.A. Effect of Magnetized Water on Workability and Compressive Strength of Concrete. *Procedia Eng.* **2017**, *193*, 494–500. [CrossRef]
81. Keshta, M.M.; Elshikh, M.M.Y.; Abd Elrahman, M.; Youssf, O. Utilizing of Magnetized Water in Enhancing of Volcanic Concrete Characteristics. *J. Compos. Sci.* **2022**, *6*, 320. [CrossRef]
82. Inaba, H.; Saitou, T.; Tozaki, K.I.; Hayashi, H. Effect of the Magnetic Field on the Melting Transition of H₂O and D₂O Measured by a High Resolution and Supersensitive Differential Scanning Calorimeter. *J. Appl. Phys.* **2004**, *96*, 6127–6132. [CrossRef]
83. Su, N.; Wu, Y.H.; Mar, C.Y. Effect of Magnetic Water on the Engineering Properties of Concrete Containing Granulated Blast-Furnace Slag. *Cem. Concr. Res.* **2000**, *30*, 599–605. [CrossRef]
84. Su, N.; Wu, C.F. Effect of Magnetic Field Treated Water on Mortar and Concrete Containing Fly Ash. *Cem. Concr. Compos.* **2003**, *25*, 681–688. [CrossRef]
85. Gholhaki, M.; Kheyroddin, A.; Hajforoush, M.; Kazemi, M. An Investigation on the Fresh and Hardened Properties of Self-Compacting Concrete Incorporating Magnetic Water with Various Pozzolanic Materials. *Constr. Build. Mater.* **2018**, *158*, 173–180. [CrossRef]
86. Wang, Y.; Wang, X.; Yang, Z. Study on Impermeability Mechanism of Magnetic Water Concrete. *Appl. Mech. Mater.* **2011**, *99–100*, 745–748. [CrossRef]
87. Ghorbani, S.; Ghorbani, S.; Tao, Z.; de Brito, J.; Tavakkolizadeh, M. Effect of Magnetized Water on Foam Stability and Compressive Strength of Foam Concrete. *Constr. Build. Mater.* **2019**, *197*, 280–290. [CrossRef]
88. Ahmed, S.M. Effect of Magnetic Water on Engineering Properties of Concrete. *Al-Rafidain Eng. J. (AREJ)* **2009**, *17*, 71–82. [CrossRef]
89. Ghorbani, S.; Sharifi, S.; Rokhsarpour, H.; Shoja, S.; Gholizadeh, M.; Rahmatabad, M.A.D.; de Brito, J. Effect of Magnetized Mixing Water on the Fresh and Hardened State Properties of Steel Fibre Reinforced Self-Compacting Concrete. *Constr. Build. Mater.* **2020**, *248*, 118660. [CrossRef]
90. Ghorbani, S.; Ghorbani, S.; Elmi, A.; Soleimani, V.; Taji, I.; Mohammadi-Khatami, M.; Tavakkolizadeh, M.; de Brito, J. Simultaneous Effect of Granite Waste Dust as Partial Replacement of Cement and Magnetized Water on the Properties of Concrete Exposed to NaCl and H₂SO₄ Solutions. *Constr. Build. Mater.* **2021**, *288*, 123064. [CrossRef]
91. Ebrahimi Jouzdani, B.; Reisi, M. Effect of Magnetized Water Characteristics on Fresh and Hardened Properties of Self-Compacting Concrete. *Constr. Build. Mater.* **2020**, *242*, 118196. [CrossRef]
92. Ghorbani, S.; Mohammadi-Khatami, M.; Ghorbani, S.; Elmi, A.; Farzan, M.; Soleimani, V.; Negahban, M.; Tam, V.W.Y.; Tavakkolizadeh, M. Effect of Magnetized Water on the Fresh, Hardened and Durability Properties of Mortar Mixes with Marble Waste Dust as Partial Replacement of Cement. *Constr. Build. Mater.* **2021**, *267*, 121049. [CrossRef]
93. Ahmed, H.I. Behavior of Magnetic Concrete Incorporated with Egyptian Nano Alumina. *Constr. Build. Mater.* **2017**, *150*, 404–408. [CrossRef]
94. Keshta, M.M.; Yousry Elshikh, M.M.; Kaloop, M.R.; Hu, J.W.; ELMohsen, I.A. Effect of Magnetized Water on Characteristics of Sustainable Concrete Using Volcanic Ash. *Constr. Build. Mater.* **2022**, *361*, 129640. [CrossRef]
95. Salehi, H.; Mazloom, M. Opposite Effects of Ground Granulated Blast-Furnace Slag and Silica Fume on the Fracture Behavior of Self-Compacting Lightweight Concrete. *Constr. Build. Mater.* **2019**, *222*, 622–632. [CrossRef]
96. Barham, W.S.; Albiss, B.; Lataifeh, O. Influence of Magnetic Field Treated Water on the Compressive Strength and Bond Strength of Concrete Containing Silica Fume. *J. Build. Eng.* **2021**, *33*, 101544. [CrossRef]
97. Al-Maliki, A.A.K.; Aswed, K.K.; Abraheem, A.K. Properties of Concrete with Magnetic Mixing Water. *AIP Conf. Proc.* **2020**, *2213*, 020146. [CrossRef]
98. Ahmed, S.M.; Manar, D.F. Effect of Static Magnetic Field Treatment on Fresh Concrete and Water Reduction Potential. *Case Stud. Constr. Mater.* **2021**, *14*, e00535. [CrossRef]
99. Ngene, B.; Bamigboye, G.; Agomo, C.; Eneh, K.; Olajide, O. Magnetic field treated water influence on structural concrete elements: Environmental issues of concern. In *Interdependence between Structural Engineering and Construction Management*; Ozevin, D., Ataei, H., Modares, M., Gurgun, A., Yazdani, S., Singh, A., Eds.; ISEC Press: Fargo, ND, USA, 2019. Available online: https://www.isec-society.org/ISEC_PRESS/ISEC_10/pdf/MAT-38.pdf (accessed on 20 December 2023).
100. Wei, H.; Wang, Y.; Luo, J. Influence of Magnetic Water on Early-Age Shrinkage Cracking of Concrete. *Constr. Build. Mater.* **2017**, *147*, 91–100. [CrossRef]
101. Sun, Y.; Zhang, P.; Hu, J.; Liu, B.; Yang, J.; Liang, S.; Xiao, K.; Hou, H. A Review on Microwave Irradiation to the Properties of Geopolymers: Mechanisms and Challenges. *Constr. Build. Mater.* **2021**, *294*, 123491. [CrossRef]
102. Zhang, H.; Wei, W.; Shao, Z.; Qiao, R. The Investigation of Concrete Damage and Recycled Aggregate Properties under Microwave and Conventional Heating. *Constr. Build. Mater.* **2022**, *341*, 127859. [CrossRef]
103. Wei, W.; Shao, Z.; Qiao, R.; Chen, W.; Zhang, P.; Cheng, J. Workability and Mechanical Properties of Microwave Heating for Recovering High Quality Aggregate from Concrete. *Constr. Build. Mater.* **2021**, *276*, 122237. [CrossRef]
104. Pan, Y.; Zhang, Y.; Li, S. Effects of Isothermal Microwave Curing on Steel Fibre-Reinforced Reactive Powder Concrete: Strength, Microstructure and Hydration Products. *Constr. Build. Mater.* **2021**, *302*, 124435. [CrossRef]

105. Tang, T.; Cai, L.; You, K.; Liu, M.; Han, W. Effect of Microwave Pre-Curing Technology on Carbide Slag-Fly Ash Autoclaved Aerated Concrete (CS-FA AAC): Porosity Rough Body Formation, Pore Characteristics and Hydration Products. *Constr. Build. Mater.* **2020**, *263*, 120112. [[CrossRef](#)]
106. Li, Y.; Yu, J.; Cao, Z.; He, P.; Liu, Q.; Han, X.; Wan, Y. Preparation and Application of Novel Microcapsules Ruptured by Microwave for Self-Healing Concrete. *Constr. Build. Mater.* **2021**, *304*, 124616. [[CrossRef](#)]
107. Ma, G.; Sun, J.; Aslani, F.; Huang, Y.; Jiao, F. Review on Electromagnetic Wave Absorbing Capacity Improvement of Cementitious Material. *Constr. Build. Mater.* **2020**, *262*, 120907. [[CrossRef](#)]
108. Luo, S.; Zhao, M.; Jiang, Z.; Liu, S.; Yang, L.; Mao, Y.; Pan, C. Microwave Preparation and Carbonation Properties of Low-Carbon Cement. *Constr. Build. Mater.* **2022**, *320*, 126239. [[CrossRef](#)]
109. Makul, N. Innovative Hybrid Curing Method for Accelerating the Strength of High-Performance Cement Paste Using Microwave Heating Coupling with Low-Pressure Processing. *Constr. Build. Mater.* **2016**, *105*, 245–252. [[CrossRef](#)]
110. Abu-Saleem, M.; Zhuge, Y.; Hassanli, R.; Ellis, M.; Rahman, M.M.; Levett, P. Microwave Radiation Treatment to Improve the Strength of Recycled Plastic Aggregate Concrete. *Case Stud. Constr. Mater.* **2021**, *15*, e00728. [[CrossRef](#)]
111. Chen, W.; Shao, Z.; Wei, W.; Zhang, P.; Hong, Y. Properties of Concrete Incorporating Microwave Treated Coarse Aggregate: An Experimental Study. *Structures* **2021**, *33*, 693–702. [[CrossRef](#)]
112. Makul, N.; Rattanadecho, P.; Agrawal, D.K. Microwave Curing at an Operating Frequency of 2.45 GHz of Portland Cement Paste at Early-Stage Using a Multi-Mode Cavity: Experimental and Numerical Analysis on Heat Transfer Characteristics. *Int. Commun. Heat. Mass. Transf.* **2010**, *37*, 1487–1495. [[CrossRef](#)]
113. Xiao, Q.; Long, G.; Feng, R.; Zeng, X.; Dong, R.; Xiang, Y.; Yang, K. Effect of Alternating Current Field on Rheology of Fresh Cement-Based Pastes. *J. Build. Eng.* **2022**, *48*, 103771. [[CrossRef](#)]
114. Liu, X.; Zhao, Y.; Wei, Z.; Zhang, D. Microwave Absorption Enhancement of Asphalt Concrete with SiC-Fe₃O₄ Mixtures Modifier. *Constr. Build. Mater.* **2020**, *254*, 119209. [[CrossRef](#)]
115. Wang, F.; Zhu, H.; Shu, B.; Li, Y.; Gu, D.; Gao, Y.; Chen, A.; Feng, J.; Wu, S.; Liu, Q.; et al. Microwave Heating Mechanism and Self-Healing Performance of Asphalt Mixture with Basalt and Limestone Aggregates. *Constr. Build. Mater.* **2022**, *342*, 127973. [[CrossRef](#)]
116. Buttress, A.J.; Jones, D.A.; Dodds, C.; Dimitrakis, G.; Campbell, C.J.; Dawson, A.; Kingman, S.W. Understanding the Scabbling of Concrete Using Microwave Energy. *Cem. Concr. Res.* **2015**, *75*, 75–90. [[CrossRef](#)]
117. Tinoco, I.V.; Pinto, R.C.d.A. Evaluation of Stiffness Loss of Reinforced Concrete Beams Using the Diffuse Ultrasound Method. *Ultrasonics* **2021**, *117*, 106540. [[CrossRef](#)] [[PubMed](#)]
118. Rattanadecho, P.; Suwannapum, N.; Chatveera, B.; Atong, D.; Makul, N. Development of Compressive Strength of Cement Paste under Accelerated Curing by Using a Continuous Microwave Thermal Processor. *Mater. Sci. Eng. A* **2008**, *472*, 299–307. [[CrossRef](#)]
119. Zhang, P.; Wei, W.; Shao, Z. Multifield Coupling Study on Random Aggregate Concrete under Microwave Irradiation. *Constr. Build. Mater.* **2022**, *318*, 126025. [[CrossRef](#)]
120. Leung, C.K.Y.; Pheeraphan, T. Microwave Curing of Portland Cement Concrete: Experimental Results and Feasibility for Practical Applications. *Constr. Build. Mater.* **1995**, *9*, 67–73. [[CrossRef](#)]
121. Trigos, L.; Escavy, J.I.; Gallego, J.; Gulisano, F. Natural Factors Related to the Differential Heating of Aggregates Exposed to Microwaves. *Constr. Build. Mater.* **2022**, *314*, 125654. [[CrossRef](#)]
122. Wang, Z.; Bai, E.; Huang, H.; Wang, T.; Sun, H. Study on the Electromagnetic Property and Microwave Heating Efficiency of Concrete with Magnetite Aggregate. *Constr. Build. Mater.* **2022**, *342*, 128080. [[CrossRef](#)]
123. Qiu, Q. A State-of-the-Art Review on the Carbonation Process in Cementitious Materials: Fundamentals and Characterization Techniques. *Constr. Build. Mater.* **2020**, *247*, 118503. [[CrossRef](#)]
124. Yang, Z.; Xie, Y.; He, J.; Zeng, X.; Ma, K.; Long, G. Experimental Investigation on Mechanical Strength and Microstructure of Cement Paste by Electric Curing with Different Voltage and Frequency. *Constr. Build. Mater.* **2021**, *299*, 123615. [[CrossRef](#)]
125. Zhang, T.; Wang, J.; Feng, J.; Liu, Y.; Suo, R.; Ma, Q.; Sun, J. Effects of Ultrasonic–Microwave Combination Treatment on the Physicochemical, Structure and Gel Properties of Myofibrillar Protein in *Penaeus Vannamei* (*Litopenaeus Vannamei*) Surimi. *Ultrason. Sonochem.* **2022**, *90*, 106218. [[CrossRef](#)] [[PubMed](#)]
126. Pengju, Z.; Wei, W.; Zhushan, S.; Rujia, Q. Effect of Moisture on Concrete Damage and Aggregate Recycling under Microwave Irradiation. *J. Build. Eng.* **2022**, *46*, 103741. [[CrossRef](#)]
127. Cheng, J.; Shao, Z.; Xu, T.; Wei, W.; Qiao, R.; Yuan, Y. Experimental Research on Sintering Construction Spoil Bricks Based on Microwave Heating Technology. *Environ. Sci. Pollut. Res.* **2021**, *28*, 69367–69380. [[CrossRef](#)] [[PubMed](#)]
128. Zhou, F.; Pan, G.; Meng, H.; Mi, R. Effect of Secondary Curing on the Performance of Microwave Cured Concrete. *Constr. Build. Mater.* **2022**, *330*, 127256. [[CrossRef](#)]
129. Kong, Y.; Wang, P.; Liu, S.; Gao, Z. Hydration and Microstructure of Cement-Based Materials under Microwave Curing. *Constr. Build. Mater.* **2016**, *114*, 831–838. [[CrossRef](#)]
130. Wei, W.; Shao, Z.; Qiao, R.; Chen, W.; Zhou, H.; Yuan, Y. Recent Development of Microwave Applications for Concrete Treatment. *Constr. Build. Mater.* **2021**, *269*, 121224. [[CrossRef](#)]
131. Muthukrishnan, S.; Ramakrishnan, S.; Sanjayan, J. Technologies for Improving Buildability in 3D Concrete Printing. *Cem. Concr. Compos.* **2021**, *122*, 104144. [[CrossRef](#)]

132. Xiao, Y.; Shao, Z.; Wei, W.; Han, Y.; Jiang, Y.; Chai, S.; Chen, X.; Zong, Z. Effect of Microwave Pretreatment on Mechanical Behavior of Concrete and Aggregate Recovery. *Constr. Build. Mater.* **2023**, *387*, 131647. [[CrossRef](#)]
133. Behnood, A.; Olek, J.; Glinicki, M.A. Predicting compressive strength of recycled concrete aggregate using M5' model. In *Brittle Matrix Composites 11, Proceedings of the 11th International Symposium on Brittle Matrix Composites, Warsaw, Poland, 28–30 September 2015*; IPPT PAN: Warsaw, Poland, 2015; pp. 381–391.
134. Chindaprasirt, P.; Rattanasak, U.; Taebuanhuad, S. Role of Microwave Radiation in Curing the Fly Ash Geopolymer. *Adv. Powder Technol.* **2013**, *24*, 703–707. [[CrossRef](#)]
135. Choi, H.; Koh, T.; Choi, H.; Hama, Y. Performance Evaluation of Precast Concrete Using Microwave Heating Form. *Materials* **2019**, *12*, 1113. [[CrossRef](#)] [[PubMed](#)]
136. Leung, C.K.Y.; Pheeraphan, T. Determination of Optimal Process for Microwave Curing of Concrete. *Cem. Concr. Res.* **1997**, *27*, 463–472. [[CrossRef](#)]
137. Zhang, J.; Yu, R.; Shui, Z.; Liu, K. Hydration Kinetics and Microstructure Development of Ultra-High Performance Concrete (UHPC) Subjected to Microwave Pre-Curing. *Cem. Concr. Compos.* **2022**, *129*, 104484. [[CrossRef](#)]
138. Korpa, A.; Trettin, R. Very High Early Strength of Ultra-High Performance Concrete Containing Nanoscale Pozzolans Using the Microwave Heat Curing Method. *Adv. Cem. Res.* **2008**, *20*, 175–184. [[CrossRef](#)]
139. Gao, Z.; He, Y.; Li, M.; Jiang, M.; Shen, J. Impacts of Microwave on Hydration Evolution of Portland Cement in the Perspective of Composition and Microstructure of Hydrates. *Constr. Build. Mater.* **2022**, *360*, 129569. [[CrossRef](#)]
140. Kong, Y.; Liu, S.; Wang, P. Effects of Microwave Curing on the Compressive Strength Development and Hydration of Cement-Granulated Blast Furnace Slag Composite System. *Constr. Build. Mater.* **2021**, *270*, 121432. [[CrossRef](#)]
141. Cheah, C.B.; Tan, L.E.; Ramli, M. Recent Advances in Slag-Based Binder and Chemical Activators Derived from Industrial by-Products—A Review. *Constr. Build. Mater.* **2021**, *272*, 121657. [[CrossRef](#)]
142. Ribeiro, D.V.; Paula, G.R.; Morelli, M.R. Use of Microwave Oven in the Calcination of MgO and Effect on the Properties of Magnesium Phosphate Cement. *Constr. Build. Mater.* **2019**, *198*, 619–628. [[CrossRef](#)]
143. Wang, X.; Li, Q.; Lai, H.; Peng, Y.; Xu, S. Broadband Microwave Absorption Enabled by a Novel Carbon Nanotube Gratings/Cement Composite Metastructure. *Compos. B Eng.* **2022**, *242*, 110071. [[CrossRef](#)]
144. Sun, W.; Wu, D.; Liu, H.; Qu, C. Thermal, Mechanical and Ultrasonic Properties of Cemented Tailings Backfill Subjected to Microwave Radiation. *Constr. Build. Mater.* **2021**, *313*, 125535. [[CrossRef](#)]
145. Wu, D.; Sun, W.; Liu, S.; Qu, C. Effect of Microwave Heating on Thermo-Mechanical Behavior of Cemented Tailings Backfill. *Constr. Build. Mater.* **2021**, *266*, 121180. [[CrossRef](#)]
146. Sun, W.; Wu, D.; Xu, W.; Ma, L.; Cao, J.; Chen, J. Coupled Electromagnetic Heat Transfer Model for Cemented Tailings Backfill Cured by Microwave Energy. *Constr. Build. Mater.* **2022**, *342*, 128014. [[CrossRef](#)]
147. Li, S.; Gao, X. Acceleration Mechanism of Nonisothermal Microwave Heating on Strength Development of Mortar. *Compos. Struct.* **2022**, *279*, 114765. [[CrossRef](#)]
148. Qin, H.; Wei, W.; Hang Hu, Y. Synergistic Effect of Graphene-Oxide-Doping and Microwave-Curing on Mechanical Strength of Cement. *J. Phys. Chem. Solids* **2017**, *103*, 67–72. [[CrossRef](#)]
149. Wang, Y.; Luo, S.; Yang, L.; Ding, Y. Microwave Curing Cement-Fly Ash Blended Paste. *Constr. Build. Mater.* **2021**, *282*, 122685. [[CrossRef](#)]
150. Guan, X.; Chen, J.; Zhu, M.; Gao, J. Performance of Microwave-Activated Coal Gangue Powder as Auxiliary Cementitious Material. *J. Mater. Res. Technol.* **2021**, *14*, 2799–2811. [[CrossRef](#)]
151. Akinyemi, A.B.; Omoniyi, E.T.; Onuzulike, G. Effect of Microwave Assisted Alkali Pretreatment and Other Pretreatment Methods on Some Properties of Bamboo Fibre Reinforced Cement Composites. *Constr. Build. Mater.* **2020**, *245*, 118405. [[CrossRef](#)]
152. Wei, W.; Shao, Z.; Zhang, P.; Chen, W.; Qiao, R.; Yuan, Y. Experimental Assessment of Microwave Heating Assisted Aggregate Recycling from Dried and Saturated Concrete. *Mater. Struct.* **2021**, *54*, 142. [[CrossRef](#)]
153. Choi, H.; Kitagaki, R.; Noguchi, T.; Tsujino, M.; Masaki, T.; Kanematsu, M.; Maruyama, I.; Dosho, Y.; Ogawa, H.; Nawa, T.; et al. Effective Recycling of Surface Modification Aggregate Using Microwave Heating. *J. Adv. Concr. Technol.* **2014**, *12*, 34–45. [[CrossRef](#)]

Disclaimer/Publisher's Note: The statements, opinions and data contained in all publications are solely those of the individual author(s) and contributor(s) and not of MDPI and/or the editor(s). MDPI and/or the editor(s) disclaim responsibility for any injury to people or property resulting from any ideas, methods, instructions or products referred to in the content.